ICARUS 109, 221–240 (1994)

A Comparison of Lorentz, Planetary Gravitational, and Satellite Gravitational Resonances

DOUGLAS P. HAMILTON[1]

Department of Astronomy, Cornell University, Ithaca NY 14853
E-mail:hamilton@eu1.mpi-hd.mpg.de

Received October 7, 1993; revised March 8, 1994

We consider a charged dust grain whose orbital motion is dominated by a planet's point-source gravity, but perturbed by higher-order terms in the planet's gravity field as well as by the Lorentz force arising from an asymmetric planetary magnetic field. Perturbations to Keplerian orbits due to a nonspherical gravity field are expressed in the traditional way: in terms of a disturbing function which can be expanded in a series of spherical harmonics (W. M. Kaula, 1966, *Theory of Satellite Geodesy*, Blaisdell, Waltham, MA). In order to calculate the electromagnetic perturbation, we first write the Lorentz force in terms of the orbital elements and then substitute it into Gauss' perturbation equations. This procedure is analogous to the derivation of gravitational disturbing functions, except, since the Lorentz force has no associated potential, the perturbation of each orbital element must be calculated separately. We use our result to derive strengths of Lorentz resonances and elucidate their properties. In particular, we compare Lorentz resonances to two types of gravitational resonances: those arising from periodic tugs of a satellite and those due to the attraction of an arbitrarily shaped planet.

We find that Lorentz resonances share numerous properties with their gravitational counterparts and show, using simple physical arguments, that several of these patterns are fundamental, applying not only to our expansions, but to all quantities expressed in terms of orbital elements. Some of these patterns have been previously called "d'Alembert rules" for satellite resonances. Other similarities arise because, to first-order in the perturbing force, the three problems share an integral of the motion. Yet there are also differences; for example, first-order inclination resonances exist for perturbations arising from planetary gravity and from the Lorentz force, but not for those due to an orbiting satellite. Finally, we provide a heuristic treatment of a particle's orbital evolution under the influence of drag and resonant forces. Particles brought into mean-motion resonances experience either trapping or resonant "jumps," depending on the direction from which the resonance is approached. We show that this behavior does not depend on the details of the perturbing force but rather is fundamental to all mean-motion resonances.

[1] Current address: Max Planck Institut für Kernphysik, Postfach 103980, 69029 Heidelberg, Germany.

1. INTRODUCTION

Gravitational orbital resonances, in which the frequency of a perturbing force is commensurate with a natural orbital frequency, have fundamental importance in the Solar System. Satellites resonate with one another as in the saturnian Mimas–Tethys and Enceladus–Dione pairs as well as the famous jovian Io–Europa–Ganymede triple. At resonant locations in the main rings of Saturn, satellites cause density and bending waves, and sometimes form gaps and ringlets. Some features in the saturnian rings have even been ascribed to tiny perturbations from axially asymmetric terms in the planet's gravitational field (Franklin *et al.* 1982, Marley and Porco 1993) and at Mars these resonances may have influenced the eccentricity and inclination of Phobos (Yoder 1982). Since gravitational resonances are so common in the Solar System, might nongravitational resonances also be prevalent? This is almost certainly true; however, examples of such resonances will only be found by looking in the right places. Since nongravitational forces can compete with gravitational ones solely when particles are small, we expect these resonances for particles with radii less than a few micrometers. The faint ring systems of the giant planets are composed primarily of tiny particles and so such locales are ideal sites to seek out signs of nongravitational resonant interactions.

These signs are clearly present both in the main jovian ring (Burns *et al.* 1985) and in Saturn's E ring (Horanyi *et al.* 1992). In the former location, Lorentz (electromagnetic) resonances, which arise from Jupiter's spinning magnetic field, are capable of pumping up the eccentricity and inclination of ring particles. In particular, the transition between the main ring and the vertically extended halo occurs at a location where the ratio of the orbital frequency to the planet's spin rate is nearly 3 : 2 (Burns *et al.* 1985). Particles drifting inward and across this strong resonant location increase their inclinations by a factor of several hundred (see Schaffer and Burns 1992). The

0019-1035/94 $6.00

particles in Saturn's diffuse E ring are also in nearly resonant orbits although this time the driving force is radiation pressure instead of electromagnetism. Here perturbations of planetary gravity and electromagnetism cause an orbit's pericenter to precess at a rate nearly commensurate with the orbital motion of Saturn. Thus an orbit retains a given orientation with respect to the Sun for an extended period of time, thereby allowing radiation pressure to build up large orbital eccentricities and spread material across the full breadth of the E ring (Horanyi *et al.* 1992).

Other nongravitational resonances have also been identified, among them two types of shadow resonances (Mignard 1984, Horanyi and Burns 1991) and resonant charge variations (Burns and Schaffer 1989, Northrop *et al.* 1989). In the former, conditions change in the planetary shadow (radiation pressure and the photoelectric current shut off) which is encountered once per orbit; such orbits are thus intrinsically resonant. Shadow resonances may be responsible for the strange azimuthal asymmetry seen in the main jovian ring and in its halo (for a description of the asymmetry, see Showalter *et al.* 1987). Resonant charge variations occur when the charge on a dust grain changes with a period that is commensurate with the grain's orbital period; the termination of the photoelectric current during shadow passage provides a simple example, while another depends on variations in the current flow to a grain as its position and velocity change along its orbit.

Because gravitational resonances have been extensively studied, it is valuable when studying nongravitational effects to draw from the body of knowledge already amassed. Accordingly, the primary emphasis of this work is to explore the similarities of nongravitational and gravitational orbital resonances by comparing and contrasting their structure and effects on orbiting particles. We choose to look at two different types of gravitational resonances—those due to an orbiting satellite and those due to the "lumpiness" of an arbitrarily shaped planet—and we pick Lorentz resonances both because of their importance at Jupiter and because of their similarity to gravitational resonances (Hamilton and Burns 1993). In the interest of brevity, henceforth we adopt the following notation: LR, Lorentz resonance; SGR, satellite gravity resonance, and PGR, planetary gravity resonance. By comparing three different types of orbital resonances, we progress in understanding the traits that underlie all orbital resonances and those that are unique to particular ones.

A second goal of this paper is the mathematical characterization of the Lorentz perturbation which is useful for several applications. As noted above, Lorentz resonances are known to play a key role at the inner edge of the main jovian ring (Burns *et al.* 1985). They are also suspected of being important elsewhere, perhaps accounting for dust found over the Neptunian pole (Hamilton *et al.* 1992), causing larger inclinations in the saturnian E ring (Horani *et al.* 1992, Hamilton 1993), and accounting for curious phenomena at the corotation distance (for Jupiter, see Showalter *et al.* 1985). These resonances have been analytically treated by Schaffer and Burns (1987) and more recently by Schaffer and Burns (1992), who used a perturbed harmonic oscillator model of resonance. Here we instead follow the standard celestial mechanics approach; since gravitational perturbations have been treated in this way, similarities and differences between resonances might be more readily apparent. Furthermore, the celestial mechanics approach has several advantages over the harmonic oscillator approach, the most obvious of which is that the results of perturbations are described by slowly varying orbital elements which allow graphic visualization of orbital evolution.

The importance of Lorentz resonances in many of the above applications remains speculative because resonant strengths are poorly known; indeed, even the structure of these resonances is not well understood. In Section 2, we attempt to rectify this situation by expanding the Lorentz force out to second order in small quantities e and i. In Section 3, we compare SGRs, PGRs, and LRs and discuss underlying symmetries contained in their expansions. We add the important dissipative effects of drag forces in Section 4, following which we present our conclusions.

2. EXPANSION OF PERTURBING FORCES

2.1. Planetary Gravity

We begin by discussing perturbations to two-body motion arising from small deviations in a planetary gravity field. This well-studied problem shares many aspects with the Lorentz perturbation and, accordingly, facilitates our later discussion of that force. Because we consider only small perturbations, solutions to the full problem differ only slightly from the exact solution to the two-body problem. Accordingly, we make use of the orbital elements since these will change relatively slowly in time. The basic task then, is to write the perturbation in terms of osculating orbital elements so that the time rate of change of each of these elements can be determined. We now sketch the derivation following the comprehensive treatment of Kaula (1966).

Working in a planet-centered reference frame rotating at the planet's spin rate Ω_p, the gravitational potential Φ outside an arbitrarily shaped body can be shown to satisfy Laplace's equation, $\vec{\nabla}^2\Phi = 0$ (Danby 1988). Solving Laplace's equation leads to the standard spherical harmonic expansion of the gravitational potential,

$$\Phi = -\frac{GM_p}{R_p}\sum_{j=0}^{\infty}\left(\frac{R_p}{r}\right)^{j+1} \sum_{k=0}^{j}[C^*_{j,k}\cos(k\phi_R) + S^*_{j,k}\sin(k\phi_R)]P^k_j(\cos\theta), \quad (1)$$

where G is the gravitational constant, M_p and R_p are the planetary mass and radius, and r, θ, ϕ_R are the usual spherical coordinates defined in the rotating frame. These coordinates can be translated into the nonrotating frame by the identity $\phi_R = \phi - \lambda'$, where $\lambda' = \Omega_p t$ is the longitude of a reference point on the rotating planet. The $P^k_j(x)$ are associated Legendre functions (Kaula 1966, Schaffer and Burns 1992). Finally, the coefficients $C^*_{j,k}$ and $S^*_{j,k}$ are dimensionless quantities whose values are set by the mass distribution within the planet. To facilitate comparison of LRs and PGRs, we choose to Schmidt-normalize the gravity coefficients. (See Stern 1976 for a discussion of different normalization conventions; the appropriate formulas can also be found in Schaffer and Burns 1992.) We place asterisks on the coefficients as a reminder of this unconventional choice.

The disturbing function, i.e., the negative of Eq. (1) rewritten in terms of orbital elements, is found by converting the spherical coordinates to orbital quantities and substituting into Eq. (1); the relevant expressions [Eqs. (5)–(8) in Hamilton (1993)] allow r, θ, and ϕ to be replaced by a, e, i Ω, u, and ν. Here a and e are the semimajor axis and eccentricity of the elliptical orbit, i is the orbital inclination, and Ω is the longitude of the ascending node; the argument of latitude, u, and the true anomaly, ν, vary rapidly and nonlinearly in time (Fig. 1). We therefore replace these latter two quantities with the longitude of pericenter ϖ, which changes slowly, and the mean longitude of the particle λ, which varies nearly linearly in time. In addition, this choice causes all reference angles to be measured from the same zero-point in space which makes the symmetries of the expansion most apparent (see Section 3.1 below). The elements employed in our expansions are therefore: a, e, i, Ω, ϖ, and λ.

We eliminate the argument of latitude with the expression

$$u = \varpi - \Omega + \nu \quad (2)$$

(Fig. 1), leaving only the true anomaly ν, which always appears inside trigonometric functions, to be translated. Because expressions relating cos ν and sin ν to trigonometric functions of the mean anomaly M are available (e.g., Smart 1953, p. 41), we proceed by using multiple-angle identities to first write our series (Eq. (1)) in terms of sums and products of cos ν and sin ν. We do this using a symbolic algebra program (MACSYMA), although with care it can be done analytically (Kaula 1966). Next the substitutions for cos ν and sin ν are employed; these expressions are complicated, involving Bessel functions and their derivatives, but can be reduced to the form $\Sigma_j B_j e^j \cos(jM)$, where the B_j are constants (Smart 1953, p. 41). These expressions converge only for $e < 0.66$, a constraint of little importance since most applications are to low-eccentricity orbits. Finally, we complete the transformation to our orbital elements by replacing M via the identity $M = \lambda - \varpi$.

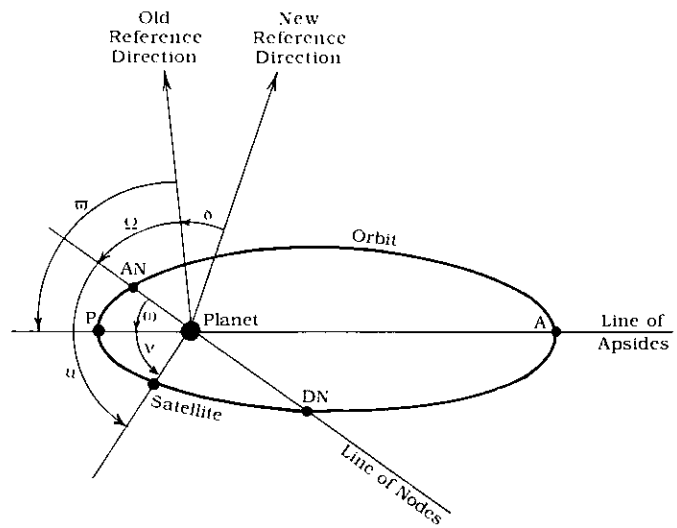

FIG. 1. Orbital elements. The symbols A and P stand for apoapse and periapse, respectively, while AN and DN refer to the ascending and descending nodes. Longitude angles (e.g., λ, ϖ, and Ω) are measured from a specified reference direction in space. Node angles (e.g., Ω) are measured to the ascending node while arguments (e.g., u and w) are measured from this point. Similarly, pericenter angles (e.g., ϖ and ω) are measured to periapse while anomalies (e.g., ν) are measured from there.

The resulting expression is quite complex, containing products and quotients of infinite power series in the eccentricity. We simplify by formally multiplying and dividing the various series so that each term in the full expression contains only a single power of the eccentricity. Next, we replace all products and powers of trigonometric functions with multiple-angle expressions; these steps are computationally intensive and tedious, and therefore are best left to symbolic programs. The final result is the disturbing function, a series containing terms of the form:

$$f(a, e, i, \ldots)SC(A_\lambda\lambda + A_{\lambda'}\lambda' + A_\varpi\varpi + A_\Omega\Omega), \quad (3)$$

where SC is either sine or cosine, the A_j are integer constants, and f is function of a, e, i and the field coefficients $C^*_{j,k}$ and $S^*_{j,k}$. Readers interested in more explicit analytic results for the disturbing function relevant to planetary gravity fields should consult Section 3.3 of Kaula (1966).

TABLE I
Orbital Perturbation Due to Planetary Gravity

Ψ									
A_λ	$A_{\lambda'}$	A_ϖ	A_Ω	$(dn/dt)^a$	$(de/dt)^a$	$(di/dt)^a$	$(d\Omega/dt)^b$	$(d\varpi/dt)^b$	$(d\varepsilon/dt)^b$
						$C^*_{2,2}$			
4	−2	−2	0	$204ne^2$	$-34e$	0	0	34	0
3	−2	−1	0	$63ne$	-7	0	0	$7/e$	0
2	−2	0	0	$12n$	$2e$	$2i$	−2	−10	12
1	−2	1	0	$-3ne$	-1	0	0	$-1/e$	0
0	−2	0	2	0	0	$2i$	2	0	0

[a] Multiply by $n(\sqrt{3}/4)C^*_{2,2}(R_p/a)^2 \sin\Psi$.
[b] Multiply by $n(\sqrt{3}/4)C^*_{2,2}(R_p/a)^2 \cos\Psi$.

						$C^*_{3,2}$			
				$(dn/dt)^c$	$(de/dt)^c$	$(di/dt)^c$	$(d\Omega/dt)^d$	$(d\varpi/dt)^d$	$(d\varepsilon/dt)^d$
4	−2	−1	−1	$-60nei$	$5i$	$5e$	$5e/i$	$5i/e$	0
3	−2	0	−1	$-9ni$	0	1	$1/i$	0	0
2	−2	1	−1	$6nei$	i	$-e$	$-e/i$	$-i/e$	0
2	−2	−1	1	$18nei$	$-3i$	$3e$	$-3e/i$	$-3i/e$	0
1	−2	0	1	$3ni$	0	1	$-1/i$	0	0
0	−2	1	1	0	i	e	$-e/i$	$-i/e$	0

[c] Multiply by $n(\sqrt{15}/4)C^*_{3,2}(R_p/a)^3 \cos\Psi$.
[d] Multiply by $n(\sqrt{15}/4)C^*_{3,2}(R_p/a)^3 \sin\Psi$.

Note. The second-order expansion of perturbations due to the $C^*_{2,2}$ and $C^*_{3,2}$ components of the planetary gravitational field. The first column contains the resonant argument, $\Psi = A_\lambda\lambda + A_{\lambda'}\lambda' + A_\varpi\varpi + A_\Omega\Omega$ [see Eqs. (3) and (11)]. When the disturbing function is expanded to second-order in the small quantities (e and i), (dn/dt) is given to second order, (de/dt) and (di/dt) to first order, and the angular quantities $(d\Omega/dt)$, $(d\varpi/dt)$, and $(d\varepsilon/dt)$ to zeroth order. The response for the $S^*_{2,2}$ and $S^*_{3,2}$ components (Eq. (1)) are obtained from these by the transformation $C^* \to S^*$ and $\Psi \to \Psi - \pi/2$. Section 4.1 gives an example of how to use this table.

We wish to compare these results with those that arise from the Lorentz force considered in the next section, but because a disturbing function cannot be defined for the Lorentz force, we must derive time rates of change of the orbital elements in both cases. These rates are obtained by inserting the disturbing function into Eq. (11.9.9) from Danby (1988), which gives six new series, one for the rate of change of each orbital element, each of which contains terms of the form of Eq. (3). We use expressions for dn/dt, de/dt, di/dt, $d\Omega/dt$, $d\varpi/dt$, and $d\varepsilon/dt$ where the mean motion is given by

$$n = \left(\frac{GM_p}{a^3}\right)^{1/2}. \tag{4}$$

The variable $d\varepsilon/dt$ encapsulates all perturbative changes to a particle's orbital mean motion; it is equivalent to Danby (1988) from $d\varepsilon_1/dt$, and satisfies $d\varepsilon/dt = d\lambda/dt - n$. To facilitate the comparison of inclination and eccentricity resonances, we Taylor-expand the six series in e and i and truncate so that only terms second-order in small quantities remain. Our results for selected quadrupole and octupole components of the planetary gravity field are presented in Table I. Many of the patterns seen in Table I [e.g., the similarity of the coefficients of the time rates of change of the eccentricity (inclination) and the pericenter (node)] follow from the fact that these expressions are derived from a single disturbing function.

2.2 The Lorentz Force

In addition to planetary gravity, a charged dust grain is influenced by the Lorentz force arising from the planet's rotating magnetic field. Close in, the magnetic field $\mathbf{B}$ rotates at the planet's constant spin rate $\mathbf{\Omega}_p$. In a frame rotating at this rate, the magnetic field is constant in time and the Lorentz force is given by

$$\mathbf{F}_{EM} = \frac{q}{c}(\mathbf{v}_{rel} \times \mathbf{B}), \tag{5}$$

where q is the charge on the grain, c is the speed of light in vacuum, and

$$\mathbf{v}_{rel} = \mathbf{v} - (\mathbf{\Omega}_p \times \mathbf{r}) \tag{6}$$

is the velocity relative to the magnetic field, with $\mathbf{v}$ as the Kepler velocity in the nonrotating frame.

When describing a magnetic field evaluated in a current-free region ($\mathbf{J} \sim \vec{\nabla} \times \mathbf{B} = 0$), the only remaining constraint that must be satisfied is Maxwell's equation $\vec{\nabla} \cdot \mathbf{B} = 0$ (Stern 1976). If $\mathbf{B} = -\vec{\nabla}\Phi_{\text{mag}}$, $\vec{\nabla} \times \mathbf{B} = 0$ is automatically satisfied, and $\vec{\nabla}^2\Phi_{\text{mag}} = 0$ with solutions like Eq. (1) above. Hence

$$\mathbf{B} = -R_p \vec{\nabla} \sum_{j=1}^{\infty} \left(\frac{R_p}{r}\right)^{j+1} \sum_{k=0}^{j} [g_{j,k} \cos(k\phi_R) + h_{j,k} \sin(k\phi_R)] P_j^k(\cos\theta). \quad (7)$$

The $g_{j,k}$ and $h_{j,k}$ are planetary magnetic field coefficients with units of Gauss [Schaffer and Burns (1992) tabulate values for the giant planets and give additional references].

We now absorb several of the constants from Eqs. (5), (6), and (7) into a single dimensionless constant representing the ratio of the Lorentz force to planetary gravity. In particular, we calculate the Lorentz force due to an aligned dipolar magnetic field on a motionless grain in the equatorial plane (i.e., $\mathbf{v} = 0$ and $\theta = 90°$) and divide by the gravitational force (both forces are radial). An advantage of this choice is that the force ratio,

$$L = \frac{q g_{1,0} R_p^3 \Omega_p}{c G M_p m_g}, \quad (8)$$

is independent of the distance from the planet. Note that the constant L depends both on properties of the grain (the charge-to-mass ratio q/m_g) and properties of the environment (planetary mass, radius, spin rate, and dipole strength).

The Lorentz force can be treated as a perturbation to gravity for grains satisfying $L \ll 1$. Assuming typical grain potentials of a few volts (e.g., Horanyi *et al.* 1992), this inequality translates to grains larger than several tenths of a micrometer in radius. For many applications, including the jovian ring (Showalter *et al.* 1987) and the saturnian E ring (Showalter *et al.* 1991), dust grains are inferred to be micrometer-sized and gravitationally dominated; hence a perturbation approach is appropriate.

Since the Lorentz force depends on velocity, it cannot be written as the gradient of a potential and thus an electromagnetic disturbing function does not exist. Therefore, in order to obtain the time rates of change of the orbital elements for a general force, we proceed as follows:

1. Resolve the force into three orthogonal components: one normal to the orbital plane, the second oriented radially, and the third perpendicular to the others.

2. Insert these components into the perturbation equations of celestial mechanics (e.g., Danby 1988, Eq. (11.5.13)).

3. Convert all quantities into orbital elements.

The first step has already been accomplished for the Lorentz force [Hamilton (1993), Eqs. (19a)–(19c): note that the magnetic field component in Eq. (19b)'s center term should be B_ϕ instead of B_θ]. Next we insert the expressions for B_r, B_θ, and B_ϕ from Eq. (7) into the force components which are in turn substituted into the perturbation equations.

Finally, we rewrite the perturbation equations in terms of our set of orbital elements; this step closely parallels that discussed above for the planetary gravity disturbing function. For each of the six perturbation equations, we first convert the spherical quantities (r, θ, ϕ) to orbital elements using Eqs. (5)–(8) from Hamilton (1993), after which we replace u and v with Ω, ϖ, and M (see Eq. (2) and the following discussion). After simplification, we are again left with a series of terms of Eq. (3)'s form. Our result for the response of a charged grain to magnetic dipole, quadrupole, octupole, and select higher-order terms, truncated to second-order in e and i, is given in Table II.

3. PROPERTIES OF THE EXPANSIONS

3.1. Orbital Symmetries

Despite the fact that the PGR and LR expansions listed in Tables I and II arise from very different perturbations, remarkably similar patterns are evident in each case. For instance, in both expansions the power of the eccentricity in a given term is related to the coefficient of the pericenter angle, A_ϖ, and the same holds for inclinations and nodes. Furthermore, in both cases, the coefficients of the angular quantities in every resonant argument Ψ sum to zero. These patterns are reminiscent of d'Alembert relations which constrain the form of SGRs, imposing symmetries that have been recognized for as long as the satellite disturbing function has been expanded. According to Brown and Shook (1933), the relation between pericenter coefficients and eccentricity powers was first discussed by d'Alembert (1754); a more complete list of symmetries present in the secular part of the disturbing function can be found in Applegate *et al.* (1986). These patterns are actually manifestations of more fundamental constraints that arise not from properties of a particular resonance, but rather from the very nature of orbital elements. In this section, we present simple physical arguments that constrain the form of *all* expressions involving orbital elements, after which we demonstrate how the constraints impose symmetries on the Fourier expansions of SGRs, PGRs, and LRs.

Any physical quantity, Q (e.g., a position, velocity, or perturbation equation, a perturbing force, the disturbing function, etc.), that is expressed in terms of orbital elements can be written as a function of many variables,

TABLE II
Orbital Perturbation Due to the Lorentz Force

Ψ				$g_{1,0}$					
A_λ	$A_{\lambda'}$	A_ϖ	A_Ω	$(dn/dt)^a$	$(de/dt)^a$	$(di/dt)^a$	$(d\Omega/dt)^b$	$(d\varpi/dt)^b$	$(d\varepsilon/dt)^b$
2	0	−2	0	$-6ne^2$	$2(1-\xi)e$	0	0	$-2(1-\xi)$	0
2	0	0	−2	$-3ni^2$	0	$(1-\xi)i$	$-(1-\xi)$	0	0
1	0	−1	0	$-3ne$	$(1-\xi)$	0	0	$-(1-\xi)/e$	0
0	0	0	0	0	0	0	$(1-\xi)$	2ξ	$-2(1-\xi)$

[a] Multiply by $nL \sin \Psi$.
[b] Multiply by $nL \cos \Psi$.

				$g_{2,0}$					
				$(dn/dt)^c$	$(de/dt)^c$	$(di/dt)^c$	$(d\Omega/dt)^d$	$(d\varpi/dt)^d$	$(d\varepsilon/dt)^d$
2	0	−1	−1	$12nei$	$-(2-\xi)i$	$-(2-3\xi)e$	$-(2-3\xi)e/i$	$-(2-\xi)i/e$	0
1	0	0	−1	$3ni$	0	$-(1-\xi)$	$-(1-\xi)/i$	0	0
0	0	1	−1	0	$-\xi i$	ξe	$\xi e/i$	$\xi i/e$	0

[c] Multiply by $nL(3/2)(g_{2,0}/g_{1,0})(R_p/a) \cos \Psi$.
[d] Multiply by $nL(3/2)(g_{2,0}/g_{1,0})(R_p/a) \sin \Psi$.

				$g_{3,0}$					
				$(dn/dt)^e$	$(de/dt)^e$	$(di/dt)^e$	$(d\Omega/dt)^f$	$(d\varpi/dt)^f$	$(d\varepsilon/dt)^f$
2	0	−2	0	$9ne^2$	$-3(1-\xi)e$	0	0	$3(1-\xi)$	0
2	0	0	−2	$6ni^2$	0	$-2(1-\xi)i$	$2(1-\xi)$	0	0
1	0	−1	0	$3ne$	$-(1-\xi)$	0	0	$(1-\xi)/e$	0
0	0	0	0	0	0	0	$-2(1-\xi)$	$(1-3\xi)$	$2(1-\xi)$

[e] Multiply by $nL(3/2)(g_{3,0}/g_{1,0})(R_p/a)^2 \sin \Psi$.
[f] Multiply by $nL(3/2)(g_{3,0}/g_{1,0})(R_p/a)^2 \cos \Psi$.

				$g_{1,1}$					
				$(dn/dt)^g$	$(de/dt)^g$	$(di/dt)^g$	$(d\Omega/dt)^h$	$(d\varpi/dt)^h$	$(d\varepsilon/dt)^h$
3	−1	−1	−1	$-45nei$	$5i$	$5(2-3\xi)e$	$5(2-3\xi)e/i$	$5i/e$	0
2	−1	0	−1	$-12ni$	0	$4(1-\xi)$	$4(1-\xi)/i$	0	0
1	1	−1	−1	$-21nei$	$(5-2\xi)i$	$(2-5\xi)e$	$(2-5\xi)e/i$	$(5-2\xi)i/e$	0
1	−1	1	−1	$9nei$	$3i$	$-3(2-\xi)e$	$-3(2-\xi)e/i$	$-3i/e$	0
1	−1	−1	1	$-15nei$	$(3+2\xi)i$	$(2-7\xi)e$	$-(2-7\xi)e/i$	$(3+2\xi)i/e$	0
0	−1	0	1	$-12ni$	0	$4(1-\xi)$	$-4(1-\xi)/i$	0	0

[g] Multiply by $nL(1/4)(g_{1,1}/g_{1,0}) \cos \Psi$.
[h] Multiply by $nL(1/4)(g_{1,1}/g_{1,0}) \sin \Psi$.

				$g_{2,1}$					
				$(dn/dt)^i$	$(de/dt)^i$	$(di/dt)^i$	$(d\Omega/dt)^j$	$(d\varpi/dt)^j$	$(d\varepsilon/dt)^j$
3	−1	−2	0	$-21ne^2$	$7(1-\xi)e$	0	0	$-7(1-\xi)$	0
3	−1	0	−2	$-9ni^2$	0	$3(1-\xi)i$	$-3(1-\xi)$	0	0
2	−1	−1	0	$-6ne$	$2(1-\xi)$	0	0	$-2(1-\xi)/e$	0
1	1	−2	0	$-9ne^2$	$3(1-\xi)e$	0	0	$-3(1-\xi)$	0
1	1	0	−2	$-9ni^2$	0	$3(1-\xi)i$	$-3(1-\xi)$	0	0
1	−1	0	0	$12ne^2$	$-4(1-\xi)e$	0	$6(1-\xi)$	$-2(1-5\xi)$	$-8(1-\xi)$
0	−1	1	0	$6ne$	$-2(1-\xi)$	0	0	$-2(1-\xi)/e$	0

[i] Multiply by $nL(\sqrt{3}/4)(g_{2,1}/g_{1,0})(R_p/a) \sin \Psi$.
[j] Multiply by $nL(\sqrt{3}/4)(g_{2,1}/g_{1,0})(R_p/a) \cos \Psi$.

				$g_{3,1}$					
				$(dn/dt)^k$	$(de/dt)^k$	$(di/dt)^k$	$(d\Omega/dt)^l$	$(d\varpi/dt)^l$	$(d\varepsilon/dt)^l$
3	−1	−1	−1	$141nei$	$-(19-10\xi)i$	$-(28-37\xi)e$	$-(28-37\xi)e/i$	$-(19-10\xi)i/e$	0
2	−1	0	−1	$24ni$	0	$-8(1-\xi)$	$-8(1-\xi)/i$	0	0
1	1	−1	−1	$93nei$	$-(19-12\xi)i$	$-(12-19\xi)e$	$-(12-19\xi)e/i$	$-(19-12\xi)i/e$	0
1	−1	1	−1	$-21nei$	$(3-10\xi)i$	$(4+3\xi)e$	$(4+3\xi)e/i$	$-(3-10\xi)i/e$	0
1	−1	−1	1	$27nei$	$3(1-4\xi)i$	$-3(4-7\xi)e$	$3(4-7\xi)e/i$	$3(1-4\xi)i/e$	0
0	−1	0	1	$24ni$	0	$-8(1-\xi)$	$8(1-\xi)/i$	0	0

[k] Multiply by $nL(\sqrt{6}/16)(g_{3,1}/g_{1,0})(R_p/a)^2 \cos \Psi$.
[l] Multiply by $nL(\sqrt{6}/16)(g_{3,1}/g_{1,0})(R_p/a)^2 \sin \Psi$.

TABLE II—*Continued*

Ψ				$g_{2,2}$					
A_λ	$A_{\lambda'}$	A_ϖ	A_Ω	$(dn/dt)^m$	$(de/dt)^m$	$(di/dt)^m$	$(d\Omega/dt)^n$	$(d\varpi/dt)^n$	$(d\varepsilon/dt)^n$
4	−2	−1	−1	$-48nei$	$4i$	$4(3-4\xi)e$	$4(3-4\xi)e/i$	$4i/e$	0
3	−2	0	−1	$-9ni$	0	$3(1-\xi)$	$3(1-\xi)/i$	0	0
2	−2	1	−1	$12nei$	$2i$	$-2(3-2\xi)e$	$-2(3-2\xi)e/i$	$-2i/e$	0
2	−2	−1	1	$-24nei$	$2(1+\xi)i$	$2(3-5\xi)e$	$-2(3-5\xi)e/i$	$2(1+\xi)i/e$	0
1	−2	0	1	$-9ni$	0	$3(1-\xi)$	$-3(1-\xi)/i$	0	0
0	−2	1	1	$-12nei$	$2(2-\xi)i$	$-2\xi e$	$2\xi e/i$	$-2(2-\xi)i/e$	0

[m] Multiply by $nL(\sqrt{3}/4)(g_{2,2}/g_{1,0})(R_p/a)\cos\Psi$.
[n] Multiply by $nL(\sqrt{3}/4)(g_{2,2}/g_{1,0})(R_p/a)\sin\Psi$.

				$g_{3,2}$					
				$(dn/dt)^o$	$(de/dt)^o$	$(di/dt)^o$	$(d\Omega/dt)^p$	$(d\varpi/dt)^p$	$(d\varepsilon/dt)^p$
4	−2	−2	0	$-15ne^2$	$5(1-\xi)e$	0	0	$-5(1-\xi)$	0
4	−2	0	−2	$-6ni^2$	0	$2(1-\xi)i$	$-2(1-\xi)$	0	0
3	−2	−1	0	$-3ne$	$(1-\xi)$	0	0	$-(1-\xi)/e$	0
2	−2	0	0	$12ne^2$	$-4(1-\xi)e$	0	$4(1-\xi)$	$-2(1-3\xi)$	$-4(1-\xi)$
1	−2	1	0	$3ne$	$-(1-\xi)$	0	0	$-(1-\xi)/e$	0
0	−2	2	0	$3ne^2$	$-(1-\xi)e$	0	0	$-(1-\xi)$	0
0	−2	0	2	$6ni^2$	0	$-2(1-\xi)i$	$-2(1-\xi)$	0	0

[o] Multiply by $nL(\sqrt{15}/4)(g_{3,2}/g_{1,0})(R_p/a)^2\sin\Psi$.
[p] Multiply by $nL(\sqrt{15}/4)(g_{3,2}/g_{1,0})(R_p/a)^2\cos\Psi$.

				$g_{3,3}$					
				$(dn/dt)^q$	$(de/dt)^q$	$(di/dt)^q$	$(d\Omega/dt)^r$	$(d\varpi/dt)^r$	$(d\varepsilon/dt)^r$
5	−3	−1	−1	$-165nei$	$11i$	$11(4-5\xi)e$	$11(4-5\xi)e/i$	$11i/e$	0
4	−3	0	−1	$-24ni$	0	$8(1-\xi)$	$8(1-\xi)/i$	0	0
3	−3	1	−1	$45nei$	$5i$	$-5(4-3\xi)e$	$-5(4-3\xi)e/i$	$-5i/e$	0
3	−3	−1	1	$-99nei$	$(5+6\xi)i$	$(28-39\xi)e$	$-(28-39\xi)e/i$	$(5+6\xi)i/e$	0
2	−3	0	1	$-24ni$	0	$8(1-\xi)$	$-8(1-\xi)/i$	0	0
1	−3	1	1	$-21nei$	$(11-6\xi)i$	$-(4+\xi)e$	$(4+\xi)e/i$	$-(11-6\xi)i/e$	0

[q] Multiply by $nL(\sqrt{10}/16)(g_{3,3}/g_{1,0})(R_p/a)^2\cos\Psi$.
[r] Multiply by $nL(\sqrt{10}/16)(g_{3,3}/g_{1,0})(R_p/a)^2\sin\Psi$.

				$g_{4,3}$					
				$(dn/dt)^s$	$(de/dt)^s$	$(di/dt)^s$	$(d\Omega/dt)^t$	$(d\varpi/dt)^t$	$(d\varepsilon/dt)^t$
5	−3	−2	0	$-39ne^2$	$13(1-\xi)e$	0	0	$-13(1-\xi)$	0
5	−3	0	−2	$-15ni^2$	0	$5(1-\xi)i$	$-5(1-\xi)$	0	0
4	−3	−1	0	$-6ne$	$2(1-\xi)$	0	0	$-2(1-\xi)/e$	0
3	−3	0	0	$36ne^2$	$-12(1-\xi)e$	0	$10(1-\xi)$	$-2(3-7\xi)$	$-8(1-\xi)$
2	−3	1	0	$6ne$	$-2(1-\xi)$	0	0	$-2(1-\xi)/e$	0
1	−3	2	0	$3ne^2$	$-(1-\xi)e$	0	0	$-(1-\xi)$	0
1	−3	0	2	$15ni^2$	0	$-5(1-\xi)i$	$-5(1-\xi)$	0	0

[s] Multiply by $nL(\sqrt{70}/16)(g_{4,3}/g_{1,0})(R_p/a)^3\cos\Psi$.
[t] Multiply by $nL(\sqrt{70}/16)(g_{4,3}/g_{1,0})(R_p/a)^3\sin\Psi$.

				$g_{4,4}$					
				$(dn/dt)^u$	$(de/dt)^u$	$(di/dt)^u$	$(d\Omega/dt)^v$	$(d\varpi/dt)^v$	$(d\varepsilon/dt)^v$
6	−4	−1	−1	$-126nei$	$7i$	$7(5-6\xi)e$	$7(5-6\xi)e/i$	$7i/e$	0
5	−4	0	−1	$-15ni$	0	$5(1-\xi)$	$5(1-\xi)/i$	0	0
4	−4	1	−1	$36nei$	$3i$	$-3(5-4\xi)e$	$-3(5-4\xi)e/i$	$-3i/e$	0
4	−4	−1	1	$-84nei$	$(3+4\xi)i$	$(25-32\xi)e$	$-(25-32\xi)e/i$	$(3+4\xi)i/e$	0
3	−4	0	1	$-15ni$	0	$5(1-\xi)$	$-5(1-\xi)/i$	0	0
2	−4	1	1	$-6nei$	$(7-4\xi)i$	$-(5-2\xi)e$	$(5-2\xi)e/i$	$-(7-4\xi)i/e$	0

[u] Multiply by $nL(\sqrt{35}/16)(g_{4,4}/g_{1,0})(R_p/a)^3\sin\Psi$.
[v] Multiply by $nL(\sqrt{35}/16)(g_{4,4}/g_{1,0})(R_p/a)^3\cos\Psi$.

Note. The second-order expansion of perturbations due to the Lorentz force with $\xi = n/\Omega_p$. All dipole, quadrupole, and octupole as well as a few of the important higher-order terms are given in separate subtables. The first column contains the resonant argument, $\Psi = A_\lambda\lambda + A_{\lambda'}\lambda' + A_\varpi\varpi + A_\Omega\Omega$ [see Eqs. (3) and (11)]. As with planetary gravity, we expand (dn/dt) to second order in e and i, (de/dt) and (di/dt) to first order, and the angular quantities $(d\Omega/dt)$, $(d\varpi/dt)$, and $(d\varepsilon/dt)$ to zeroth order. By convention, the $h_{0,k}$ are taken to be zero; the response to the other $h_{j,k}$ terms can be obtained from this table by substituting $h_{j,k}$ in for $g_{j,k}$ and subtracting $\pi/2$ from Ψ. An example illustrating the proper use of this table for the $g_{3,3}$ component is given in Eqs. (29a)–(29c) of Section 4.1.

$$Q = F(\chi_1, \chi_2, \chi_3, \ldots, \phi_1, \phi_2, \phi_3, \ldots), \tag{9}$$

some of which are longitude angles (ϕ_j) and some of which are not (χ_j). For the Lorentz perturbation (see Section 2.2 and Table II), the set of χ_j includes the quantities $\{a, e, i, L, g_{j,k}, h_{j,k}\}$, while the set of ϕ_j is simply $\{\Omega, \varpi, \lambda, \lambda'\}$. Since the longitudes are angular quantities, F must be periodic in each of them. A well-behaved periodic function can be expanded as a Fourier series in each of its cyclic variables; performing this expansion of Eq. (9) yields a series whose terms have the form

$$f(\chi_1, \chi_2, \chi_3, \ldots)\mathrm{SC}(\Psi), \tag{10}$$

where SC is either sine or cosine, the function f plays the role of an amplitude and

$$\Psi = \sum_j A_j \phi_j. \tag{11}$$

This series is summed over all possible unique sets of integer A_j's. Now, although all quantities pertaining to an arbitrary orbit may be expressed as a series with terms of the form of Eq. (10), the converse is not true; not all functions of this form represent valid physical quantities. We now discuss four constraints on the form of Eq. (9) that *all* physical quantities must obey.

The first and best-known constraint arises from the fact that all longitude angles are measured from the same reference direction, or zero-point, in space (e.g., Applegate *et al.* (1986). Because space is isotropic, the choice of reference direction is arbitrary, and hence its selection can in no way affect a given orbit or the perturbations acting on it. We choose a new zero-point of longitude by adding an angular quantity δ to each of the longitude terms and require that Eq. (9) be invariant under the transformation

$$\text{longitude angles} \rightarrow \text{longitude angles} + \delta \tag{12}$$

(Fig. 1).

Applying Eq. (12) to the specific case of a scalar Q, we find that since the invariance holds for arbitrary values of the variables χ_j and ϕ_j, the constraint applies separately to each term in the Fourier series (Eq. 10). If Q is unaltered by Eq. (12), then combining Eqs. (10)–(12) yields:

$$f(a, e, i, \ldots)\mathrm{SC}(\Psi) = f(a, \mathrm{e}, i, \ldots)\,\mathrm{SC}\left(\Psi + \delta \sum_j A_j\right). \tag{13}$$

Now since δ is arbitrary,

$$\sum_j A_j = 0. \tag{14}$$

Thus the longitude coefficients contained within each term of any scalar physical quantity must sum to zero. Notice in particular that this rule is strictly obeyed by each term of the perturbation expansions listed in Tables I and II.

Unlike the zero-point of longitude, the line of nodes for a given orbit is uniquely determined by the intersection of the orbital plane with a given reference plane. Nevertheless, it is an arbitrary choice to measure angles with respect to an orbit's ascending node rather than its descending node. If we adopt the unconventional choice of using the descending node, the following modifications must be made to the usual orbital elements:

$$\begin{aligned} \text{node angles} &\rightarrow \text{node angles} + \pi \\ \text{arguments} &\rightarrow \text{arguments} - \pi \\ i &\rightarrow -i. \end{aligned} \tag{15}$$

The first two transformations adjust the angles so that they are measured relative to the new reference point, the *descending* node (Fig. 1). As seen from descending node, the orbit dips below the reference plane in the direction of orbital motion and thus the new inclination is negative. Since the transformation merely amounts to describing the same orbit from a different reference point, as with the zero-point of longitude, no analytic expression can depend on this choice.

In an entirely analogous manner, the line of apsides is determined for an eccentric orbit, but one can measure angles from either pericenter or from apocenter. By choosing to measure from apocenter, the usual orbital elements must be modified as follows:

$$\begin{aligned} \text{periapse angles} &\rightarrow \text{periapse angles} + \pi \\ \text{anomalies} &\rightarrow \text{anomalies} - \pi \\ e &\rightarrow -e. \end{aligned} \tag{16}$$

As with the node above, the first two transformations adjust angles so that they are measured relative to the new reference point (Fig. 1). The third transformation, in which the sign of the eccentricity is reversed, is necessary so that the transformed distance and velocity components along the elliptical orbit retain their original values.

Equations (15) and (16), like Eq. (12), express general constraints that are strictly obeyed by Eq. (9) irregardless of whether that expression is scalar, vectorial, or tensorial. Applying Eqs. (15) and (16) to a scalar equation, we find that if Q is unaltered by the transformations, as are dn/dt, $d\Omega/dt$, $d\varpi/dt$, and $d\varepsilon/dt$, then the following expressions constrain the form of Eq. (10):

$$f(a, e, i, \ldots)\mathrm{SC}(\Psi) = f(a, e, -i, \ldots)\mathrm{SC}(\Psi + \pi A_\Omega) \tag{17}$$

and

$$f(a, e, i, \ldots)\mathrm{SC}(\Psi) = f(a, -e, i, \ldots)\mathrm{SC}(\Psi + \pi A_\varpi), \tag{18}$$

which reduce to

$$f(a, e, i, \ldots) = (-1)^{A_\Omega} f(a, e, -i, \ldots) \tag{19}$$

and

$$f(a, e, i, \ldots) = (-1)^{A_\varpi} f(a, -e, i, \ldots). \tag{20}$$

When Q is de/dt [di/dt], it changes sign under the transformation Eq. (16) [Eq. (15)] and an extra minus sign appears on the left-hand side of Eq. (20) [Eq. (19)]. Thus the function f is not arbitrary; indeed, it must be either even or odd in each of the variables e and i. Furthermore, the parity of f with respect to e or i determines the parity of the corresponding angular quantity's coefficient. This constraint is clearly evident for each of the entries in Tables I and II; the time derivatives of the mean motion and the angular quantities obey Eqs. (19) and (20) while de/dt and di/dt differ by a minus sign. The symmetries also require that power series expansions of f contain *all even* (or *all odd*) powers of e and i, a fact that is apparent in high-order expansions of SGRs (Murray and Harper 1993), PGRs (Kaula 1966), and LRs (Hamilton, unpublished).

The final simple constraint that we discuss arises from reflection of a system through the xy plane. One could reflect the entire physical system and demand that the laws of physics still be obeyed, but it is equivalent to reflect the coordinate system and describe the unreflected physical system from the new reference frame. We choose the latter approach since it parallels our previous discussions. Imagine, therefore, working in a reflected coordinate system in which angles are measured from the negative $\hat{\mathbf{z}}$ axis rather than the positive one (Fig. 2). The orbital elements are affected by the change since the ascending node of an orbit in the original xyz coordinate system is the descending node in the new $xy(-z)$ system. Since it is usual to measure angles to (or from) the ascending node, changing to the new system necessitates adding π to angles that measure the location of the node and subtracting π from arguments measured from that location (i.e., the first two lines of Eq. (15)). With this transformation, we succeed in describing the same orbit from the two reference frames. For SGRs, the transformation must be performed on all satellite orbits and the requirement

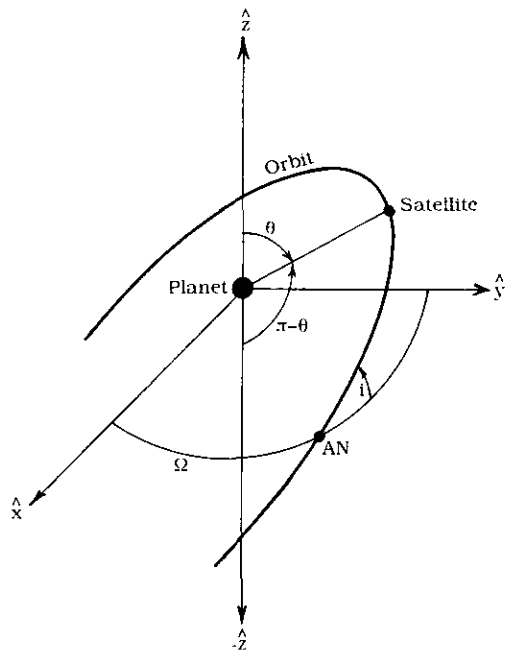

FIG. 2. An orbit seen from two coordinate systems. In the xyz system, AN marks the position of the ascending node since the polar angle θ decreases as the satellite moves away from this point (i.e., the orbit ascends above the xy reference plane). As seen from the $xy(-z)$ system, however, the polar angle is $\pi - \theta$ and AN is the *decending* node since the polar angle increases in the direction of orbital motion.

that the disturbing function, and hence Eq. (10), be unaltered by the transformation implies that the sum of the node coefficients in each term of the expansion must be even. Taken together with Eq. (19), this in turn implies the well-known result that no first-order inclination resonances exist for SGRs.

For PGRs and LRs, the gravitational and magnetic fields must also be described in the new coordinate system. Indeed, $\hat{\mathbf{z}} \rightarrow -\hat{\mathbf{z}}$ implies $\hat{\theta} \rightarrow -\hat{\theta}$, $\theta \rightarrow \pi - \theta$, and $P_j^k(\cos\theta) \rightarrow (-1)^{j+k} P_j^k(\cos\theta)$ (Fig. 2). To retain the original configuration of the gravity field, the quantity $C_{j,k}^* P_j^k(\cos\theta)$ must be unaltered and hence $C_{j,k}^* \rightarrow (-1)^{j+h} C_{j,k}^*$. With these transformations, we succeed in describing the identical problem from two different coordinate systems and, as before, the results of a perturbation cannot depend on the choice of reference frame. In the PGR expansion of the time rates of change of the orbital elements (Q), each f is proportional to one of the $C_{j,k}^*$. Since Q itself is unaltered by the change of coordinate systems, the constraint on Eq. (10) takes the form: $C_{j,k}^* \mathrm{SC}(\Psi) = (-1)^{j+k} C_{j,k}^* \mathrm{SC}(\Psi + \pi A_\Omega)$ or

$$(-1)^{A_\Omega} = (-1)^{j+k}. \tag{21}$$

For the LR expansions f is proportional to $L(g_{j,k}/g_{1,0})$, L

is unaltered by the change of coordinate systems, and $g_{j,k}$ transforms like $C^*_{j,k}$. Thus the appropriate constraint differs from Eq. (21) by a single minus sign. Summarizing our results for the three resonances, we have:

$$\begin{aligned} &\text{SGRs, Sum of node coefficients is always even;} \\ &\text{PGRs, } j + k + A_\Omega \text{ is always even;} \\ &\text{LRs, } j + k + A_\Omega \text{ is always odd.} \end{aligned} \tag{22}$$

Notice that the results for PGRs and LRs do not exclude first-order inclination resonances. In fact, first-order inclination resonances occur for PGRs when $j + k$ is odd and for LRs when $j + k$ is even (cf. $C^*_{3,2}$ term in Table I and $g_{2,2}$ term in Table II).

The constraints presented in Eqs. (14), (19), (20), and (22) account for many of the patterns seen in the expansions of SGRs, PGRs, and LRs. More patterns will be discussed below, but first we wish to stress the generality of Eqs. (12), (15), and (16) and mirror symmetry. These apply not only to SGRs, PGRs, and LRs, but to *any* possible form of an *arbitrary* perturbation. For example, each of the orbit-averaged perturbations for oblateness, radiation pressure, and electromagnetism given in Hamilton (1993) satisfy the general constraints. Moreover, the three equations hold for *all* physical quantities that are written in terms of orbital elements. This property can be especially useful for spot-checking complicated expressions. For instance, the expansions for $\sin \nu$ and $\sin E$ in terms of mean anomaly found in Danby (1988, p. 437) do not manifest the symmetry implied by Eq. (16) and hence cannot be correct; valid expressions are found in Smart (1953).

The patterns in the SGR disturbing function have been known for centuries and the fact that Eq. (14) follows from the general constraint imposed by Eq. (12) is well understood as is evident by discussions in recent publications (e.g., Applegate *et al.* 1986, Milani *et al.* 1987, Message 1991). Mirror symmetry, one of the basic precepts of modern physics, is less clearly reflected in the celestial mechanics literature. Although we note that many celestial dynamicists realize that this symmetry causes the differences between eccentricity and inclination SGRs, we have been unable to find a published derivation of this fact. We can say with certainty (near certainty), however, that the constraints that mirror symmetry imposes on LRs (PGRs) are given here for the first time. Our reasonably extensive search of both the classical and modern literature also turned up no reference to the general transformations given in Eqs. (15) and (16), nor to the simple physical arguments that we presented as proof. We conclude that these concepts are most likely new, although we cannot discount the possibility that similar ideas may have been previously published in a location unknown to us.

3.2. *The Jacobi Integral*

The properties discussed above are shared by all perturbations simply because of the nature of orbital elements. The resulting rules explain many of the patterns that are apparent in Tables I and II. Additional similarities are present because in each of the problems there is a unique rotating frame in which the perturbation is constant in time; for SGRs the frame rotates at the angular rate of perturbing satellite, while for PGRs and LRs, it rotates at the planetary spin rate. When expressed in this rotating frame, $\mathbf{F} = m\mathbf{a}$ contains both a centrifugal term and a Coriolis term. Nevertheless, a conserved quantity of the motion (energy) can be found by taking the dot product of the equation of motion with $\mathbf{v}_{\text{rel}}$ and integrating over time; for SGRs, this procedure yields the classical Jacobi constant (Danby 1988, p. 253).To zeroth-order in the perturbing force, the conserved quantity H is given by

$$H = -\frac{GM}{r} - \frac{1}{2}\Omega_p^2(x^2 + y^2) + \frac{1}{2}v_{\text{rel}}^2, \tag{23}$$

where, for SGRs, Ω_p here and below is understood to be the mean motion of the perturbing satellite. The first term is the gravitational potential energy, the second is the potential corresponding to the centrifugal force, and the final term represents the particle's kinetic energy. Because of its perpendicularity to $\mathbf{v}_{\text{rel}}$, the Coriolis force does not contribute to Eq. (23). In applying Eq. (23) to SGRs, we neglect the small contribution of the perturbing satellite which is a good approximation when one is not too close to the satellite (cf. Roy 1978, p. 129). For PGRs, we neglect the higher-order gravitational coefficients which is also a reasonable approximation. Finally, the Lorentz perturbation, like the Coriolis acceleration, is perpendicular to $\mathbf{v}_{\text{rel}}$ (see Eq. (5)) and so its term disappears when dotted with the velocity, leaving the energy integral unaltered. This is true even if the particle's charge varies with time (Horanyi and Burns 1991). Thus Eq. (23) is the exact integral of the motion for the Lorentz perturbation. We now convert this constant of the motion into orbital elements to see how it constrains the form of our expansions. This conversion was first accomplished by Tisserand (Roy 1978; Eq. (5.50)). We find

$$\frac{R_{\text{syn}}}{a} + 2\left(\frac{a}{R_{\text{syn}}}\right)^{1/2}(1 - e^2)^{1/2}\cos i = C, \tag{24}$$

where R_{syn} is the radial position of synchronous orbit and C is a constant. We use

$$\Omega_p = \left(\frac{GM_p}{R_{\text{syn}}^3}\right)^{1/2} \tag{25}$$

and Eq. (4) to replace the distances in Eq. (24) with frequencies. Since we are interested in expressing the constraint in terms of our derived time rates of change, we differentiate and obtain

$$\frac{1}{n}\left(\frac{n}{\Omega_p} - (1-e^2)^{1/2}\cos i\right)\frac{dn}{dt} - \frac{3e\cos i}{(1-e^2)^{1/2}}\left(\frac{de}{dt}\right) - 3(1-e^2)^{1/2}\sin i\left(\frac{di}{dt}\right) = 0 \quad (26)$$

which, to lowest-order in e and i, reduces to

$$3ne\frac{de}{dt} + 3ni\frac{di}{dt} + \left(1 - \frac{n}{\Omega_p}\right)\frac{dn}{dt} = 0. \quad (27)$$

Equations (26) and (27) provide a link between variations in a, e, and i which can be used in a number of applications. For example, Burns and Schaffer (1989) and Horanyi and Burns (1991) have used planar versions of Eq. (26) in electromagnetic problems to obtain de/dt when da/dt (or dn/dt) is known, while Schaffer and Burns (1992) were the first to apply a variant of Eq. (27) to elucidate properties of Lorentz resonances. The expressions can also be used to check derivations; the orbit-averaged electromagnetic expressions in Hamilton (1993), for instance, obey Eq. (26) as they must. We now discuss how Eq. (26) constrains the form of our expansions given in Tables I and II.

For any orbit, the changes in the orbital elements imposed by the full perturbation must satisfy Eq. (26). In general, many terms add together to produce these changes, but at resonant locations the effects of a single term dominate all others. At these locations, the resonant term itself must obey Eq. (26), but elsewhere it need not. The expansion of PGRs (Table I) illustrates this property nicely; only at resonance, where $n/\Omega_p \approx |A_{\lambda'}/A_\lambda|$, do single resonant terms satisfy Eq. (27). The situation for Lorentz resonances is even simpler. As can be seen in Table II, each term satisfies Eq. (27), regardless of the value of $\xi = n/\Omega_p$, and thus the cumulative perturbation automatically does too.

3.3. Additional Patterns

In the previous few sections we have discussed simple physical ideas that put strong constraints on the form of *all* resonances; here we investigate rules of a more limited scope. Some of these apply to just one type of resonance while others follow from mathematical properties of the expansions rather than from simple physical arguments.

Several additional physical rules further constrain the form of Lorentz resonances. First, the Lorentz force must vanish for a circular uninclined orbit at the synchronous distance, since there the velocity relative to the magnetic field is zero (Eq. (5)). This fact is reflected in the expansion of Table II; all dn/dt, de/dt, di/dt, and $d\varepsilon/dt$ terms disappear in the limit $n \to \Omega_p$, $e \to 0$, $i \to 0$ (cf. Hamilton 1993). The $d\Omega/dt$ and $d\varpi/dt$ terms need not vanish in this limit as these orbital elements are undefined for planar and circular orbits, respectively. Furthermore, consideration of Eqs. (5) and (6) shows that the Lorentz expansion splits into two pieces, one arising from the $\mathbf{v} \times \mathbf{B}$ component of the force (ξ terms in Table II), and one due to $(\mathbf{\Omega}_p \times \mathbf{r}) \times \mathbf{B}$ (constant terms in Table II). Since the $\mathbf{v} \times \mathbf{B}$ force can do no work in the non-rotating frame, it cannot alter the orbital energy, and hence there are no ξ terms in Table II's dn/dt entries.

Some patterns can best be explained mathematically. One such regularity seen in both Table I and Table II is that the powers of the eccentricity and inclination in the dn/dt equation equal or exceed the arguments of the corresponding angular quantities in Ψ. This property can be shown to be true by carefully following through the expansion of the perturbing forces; it stems from the fact that each appearance of a ν or u is accompanied by an e or i, respectively. Furthermore, the structure of the perturbation equations (Danby 1988, Eq. (11.5.13)) also insures that the power of e in the de/dt and $d\varpi/dt$ equations are, at most, one and two lower than A_ϖ, while the power of i in the di/dt and $d\Omega/dt$ terms follow the same pattern with respect to A_Ω. Finally, the fact that the absolute values of the numerical coefficients in the de/dt and $d\varpi/dt$ (di/dt and $d\Omega/dt$) terms are identical, at least to lowest order, also follows from the structure of the perturbation equations.

For typical resonant arguments, the equality in the patterns discussed in the above paragraph holds exactly. The only exceptions are resonances at synchronous orbit which have arguments of the form $A\lambda - A\lambda'$. Additionally, these strange resonances are the only ones that influence the $d\varepsilon/dt$ equation, although the effect is weak for LRs since $\xi \approx 1$. Examining the $2\lambda - 2\lambda'$ resonant argument (see the $C^*_{2,2}$ entries of Table I and the $g_{3,2}$ entries of Table II), we see that the gravitational version of this resonance has much more influence on the orbital elements than the Lorentz version does. This manifests the fact that the Lorentz force weakens drastically in the vicinity of synchronous orbit.

The resonant arguments of Tables I and II all have $|A_{\lambda'}| = k$, which follows directly from the fact that the gravitational and magnetic fields for the appropriate coefficients have k-fold longitudinal symmetry. This constraint, taken together with Eqs. (14) and (22) and the above discusion, allows us to predict which resonant arguments will appear for a given field coefficient. In comparing Table I's $C^*_{3,2}$ and Table II's $g_{2,2}$ entries, for example,

we see that all possible first- and second-order resonant arguments (those for which $|A_\Omega| + |A_\varpi| \leq 2$) are present. The $g_{3,2}$ entries also contain all possible arguments of order two, but a few are missing from the $C^*_{2,2}$ entries. The missing arguments are best explained by looking at the mathematical expansion of planetary gravity (Kaula 1966). Properties of the series expansions for PGRs show that all arguments with $A_\lambda = 0$ and $A_\varpi = \pm 2$ as well as those that satisfy $j - k + A_\Omega < 0$ cannot appear in the expansion. The missing term ($C^*_{2,2}: \Psi = -2\lambda' + 2\varpi$) is an example of the former constraint, while ($C^*_{2,2}: \Psi = 4\lambda - 2\lambda' - 2\Omega$)'s absence illustrates the latter.

3.4. *Global Structure; Considerations of Resonance Strength*

Although the ideas discussed above significantly constrain the structure of individual resonances, they put few restrictions on the global properties of the entire expansions. Accordingly, in this section we address the distribution and relative strengths of resonances in each of the three cases.

To a first approximation, the distributions of SGRs, PGRs, and LRs relative to synchronous orbit are almost identical because the nodal and apsidal frequencies are slow compared to the mean motions and, consequently, can be ignored when calculating rough resonance positions. For all three problems, Nth-order resonances ($N = |A_\Omega| + |A_\varpi|$) are located inside synchronous orbit when $|A_\lambda| < |A_{\lambda'}|$ and outside that position when $|A_\lambda| > |A_{\lambda'}|$. The radial location of resonance, a, is determined by

$$\frac{a}{R_{\text{syn}}} = \left(\frac{\Omega_p}{n}\right)^{2/3} = \left|\frac{A_\lambda}{A_{\lambda'}}\right|^{2/3}. \tag{28}$$

As in Section 3.2, for SGRs R_{syn} and Ω_p are understood to be the perturbing satellite's distance and mean motion, respectively. We use Eq. (28) to plot the positions of several first-order resonances ($N = 1$) and two second-order ones ($N = 2$) in Fig. 3. These resonances cluster together most tightly in the vicinity of synchronous orbit—adjacent resonances become arbitrarily close for large A_λ. Higher-order resonances behave similarly although Eq. (28) shows that they extend further from synchronous orbit than their first-order cousins.

Although resonances lie in similar positions for each perturbation, their strengths relative to one another vary depending on the details of the perturbing force. For example, each field coefficient (e.g., $g_{2,2}$) produces two first-order resonances, one inside R_{syn} ($\Psi = \lambda - 2\lambda' + \Omega$) and one outside ($\Psi = 3\lambda - 2\lambda' - \Omega$). For LRs, the strengths of these two resonances are related since, to a sign, they have identical entries (Table II); for PGRs,

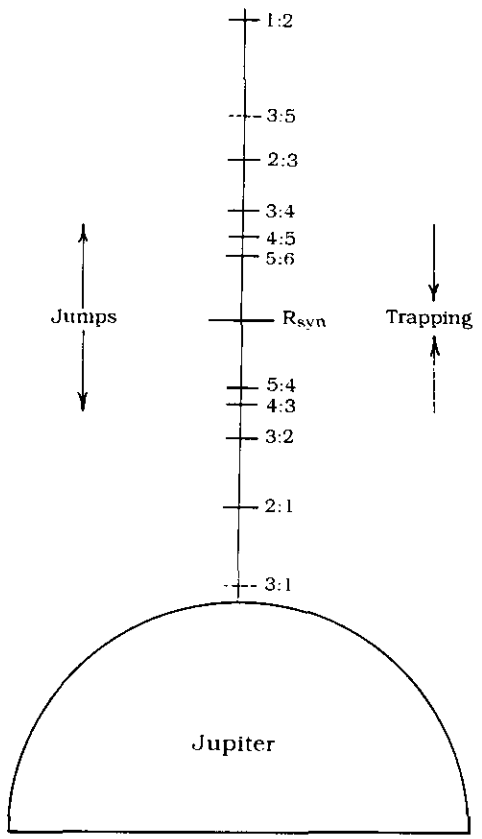

FIG. 3. Location of the several strong first-order (solid lines) and two representative second-order (dashed lines) Lorentz resonances around Jupiter. For Jupiter, $R_{\text{syn}} = 2.24$ planetary radii. The figure applies equally well to planetary gravity resonances and, if the perturbing satellite is at R_{syn}, to satellite resonances. In Section 4, we find that dust grains spiraling *toward* synchronous orbit can become trapped at resonant locations while those dragged *away* from synchronous orbit experience resonant jumps in either the inclination or eccentricity. Both of the displayed second-order resonances (3:5 and 3:1) arise from the $g_{4,3}$ component of the magnetic field (Table II). Since the second-order 1:3 resonance is found far beyond the 1:2 resonance (Eq. (28)), we see that higher-order resonances cover a broader radial range than first-order ones do.

through, the entries differ (Table I). More important, however, is the morphology of resonances in the vicinity of synchronous orbit. For SGRs, synchronous orbit is occupied by the perturbing satellite and so resonant strengths rise as this location is approached. Since resonances both increase in strength and decrease in separation as synchronous orbit is neared, it is inevitable that resonance overlap eventually occurs. At this point, single-resonance models of orbital motion are inappropriate and chaotic motions predominate; Wisdom (1980) has shown that resonance overlap occurs at a distance proportional to $\mu^{2/7}$, where μ is the satellite-to-planetary mass ratio. Unlike SGRs, PGRs and LRs tend to weaken as synchronous orbit is approached since these resonances depend on

successively larger powers of R_p/a (Fig. 3 and Tables I and II). Thus the spacing and strength effects compete, and it is not immediately obvious which dominates; Schaffer and Burns (1987), however, argue that this variety of resonance overlap does *not* occur for Lorentz resonances.

Instead, a different type of resonant overlap happens for PGRs and LRs. Just as the main energy levels of the hydrogen atom resolve into a multiplet of closely spaced levels, so a detailed examination of resonant locations reveals a similar fine structure. Each individual location (e.g., 3 : 2 in Fig. 3) resolves into a cluster of resonances with a fixed ratio $A_\lambda/A_{\lambda'}$ and different nodal and apsidal coefficients. These resonances lie at slightly different locations due to the non-zero precession rates $d\Omega/dt$ and $d\varpi/dt$ which arise primarily from the axisymmetric components of SGRs, PGRs, and LRs (e.g., the $g_{j,0}$ terms of Table II). If one ignores the resonant contributions to precession, then for SGRs and PGRs, inclination resonances lie further from synchronous orbit than eccentricity resonances; this is due to the fact that secular gravitational perturbations cause orbital nodes to regress and orbital pericenters to precess. For LRs, the situation is more complicated because both gravitational and electromagnetic perturbations influence the precession rates. In some cases, the Lorentz force can cause the opposite behavior, i.e., *nodal precession* and *apsidal regression* (see the $g_{1,0}$ and $g_{3,0}$ components of Table II). Thus inclination resonances may be closer to synchronous orbit than eccentricity resonances. Finally, since the electromagnetic precession rate depends on L, and hence on the charge-to-mass ratio of a dust grain, an ensemble of particles of different sizes will experience resonances in a range of slightly different locations. For some charge-to-mass ratios, the strong first-order inclination and eccentricity resonances are close enough to interfere with one another, leading to resonant overlap and chaos (see Fig. 5 of Schaffer and Burns 1992).

In the expansions of PGRs and LRs presented in Tables I and II, we have assumed that the gravitational and magnetic field coefficients are time-independent and thus the fields rotate as rigid objects (i.e., at a single frequency). In reality, however, these coefficients probably change slowly [cf. Levy (1989) for LRs at Jupiter] and, in some cases, even rapidly [cf. Marley (1991), Marley and Porco (1993) for PGRs at Saturn]. Unfortunately, the physics driving these changes, especially those of the magnetic field, are poorly understood, which precludes a quantitative discussion. Nevertheless, we can determine the qualitative effects of gradual changes in the fields by analogy with satellite resonances. In SGRs, the perturbing satellite has three distinct orbital frequencies: its rapid mean motion and slower nodal and apsidal precession rates. If the precession rates are suppressed, all corotation resonances (whose arguments depend on quantities of the perturber that are gradually changing) disappear from the disturbing function. In an entirely similar manner, the inclusion of slow drift frequencies to both the PGR and LR problems introduces corotation resonances that are slightly separated from the nominal resonant locations (Fig. 3).

Because corotation resonances affect only the perturbee's mean motion, they are often of minor importance. When a satellite is the perturber, however, the paired interactions of a corotation resonance and a nearby eccentricity resonance are capable of longitudinally confining ring arcs (Goldreich *et al.* 1986, Porco 1991). Thus the existence of corotation resonances in the other two cases may not be entirely academic. In particular, we suggest that similar trapping mechanisms may operate in some faint rings that are influenced by Lorentz forces.

4. COUPLING WITH DRAG FORCES

4.1. Resonant Equations

Acting alone, mean-motion resonances are capable of inducing moderately large, periodic changes in the orbital elements of nearby particles. Nonetheless, because the majority of possible orbits are far from resonant locations, resonant effects might seem to be unimportant. Not so! When coupled with a drag force, which causes secular evolution of an orbit's mean motion, the importance of resonances is greatly enhanced since drag forces will inevitably transport distant particles to resonant locations where they can be strongly perturbed. Furthermore, drag forces allow resonant perturbations to secularly change orbital eccentricities and inclinations as we will demonstrate below. Depending on the direction of the drift, drag forces acting at resonance can cause jumps in the value of e and/or i as well as resonant trapping with an associated sustained growth in those elements.

The importance of the coupling between drag forces and resonances was first recognized by Goldreich (1965), who argued that tidal drags cause satellites to evolve into, and subsequently become stably trapped in, satellite mean-motion resonances. Since then, the capture process has been reexamined (Greenberg 1973a), individual examples have been analyzed (e.g., Sinclair 1975, Greenberg 1973b), and Hamiltonian methods have been applied to the process (Peale 1976, Henrard 1982, Borderies and Goldreich 1984, Dermott *et al.* 1988, Malhotra 1991). In these next few sections we argue that particles drifting into PGRs and LRs display dynamic behavior similar to that seen at SGRs. We also illustrate how our LR expansion can be applied to the study of particular resonances.

Small particles that make up diffuse ring systems are not significantly influenced by tidal forces; instead several additional drag forces operate on these particles. Plasma and atmospheric drags arise from motion through swarms of charged and neutral molecules that corotate with the

planet; accordingly, these drags slow particles inside of R_{syn} and speed up those outside of this position. Orbital evolution, therefore, is radially away from the synchronous location. Poynting–Robertson drag arises from the asymmetric scattering and reradiation of photons (Burns *et al.* 1979) and always causes orbits to lose energy and evolve inward. Finally, resonant charge variations arise from the lag in the response of a grain's charge as its orbital motion takes it into regions with different charging currents. Depending on the plasma parameters, resonant charge variations can cause the semimajor axis to either increase or decrease (Burns and Schaffer 1989, Northrop *et al.* 1989). Although these drag forces only operate on small particles they, like tidal evolution, can bring material to resonances and influence the subsequent dynamics. The analogous process for interplanetary dust—evolution under Poynting–Robertson drag into resonances with the planets—was first recognized by Gold (1975) and later numerically studied by Gonczi *et al.* (1982). Several recent papers revisit and extend the early results (e.g., Jackson and Zook 1989, 1992, Weidenschilling and Jackson 1993, Roques *et al.* 1993, Lazzaro *et al.* 1993).

After the discussion in Section 3, it should not be surprising that LRs and PGRs behave almost identically to SGRs when coupled with a drag force. The main difference is due to the existence of strong first-order inclination-type PGRs and LRs. In fact for LRs, inclination resonances are usually stronger than the corresponding eccentricity ones (Table II). Thus, while a distribution of dust evolving through a set of SGRs might be expected to remain roughly planar due to the dominance of eccentricity-type resonances, this will not be the case for PGRs and especially LRs as the jovian halo so elegantly demonstrates (Burns *et al.* 1985). To emphasize this point, we treat a first-order inclination-type resonance in this section although the structure of the equations, and hence the resonant dynamics, is identical for an eccentricity resonance (see Table II and Hamilton and Burns 1993).

In writing a set of equations valid for the passage of a grain through an isolated resonance, we include the drag force as well as the perturbation's resonant and secular terms. We specialize the equations to the 3 : 2 first-order Lorentz inclination resource which is thought to cause the transition from the main jovian ring to its interior halo (Burns *et al.* 1985). The governing equations come from the $(g_{3,3}: \Psi = 2\lambda - 3\lambda' + \Omega)$ entry of Table II. Since a first-order inclination resonance does not strongly affect e, ϖ, and ε (see Table II), we ignore changes in these elements. Taking $\xi = n/\Omega_p \approx 3/2$, the appropriate expressions are

$$\frac{dn}{dt} = -3in^2\beta\cos(2\lambda - 3\lambda' + \Omega) + \dot{n}_{drag} \quad (29a)$$

$$\frac{di}{dt} = -\frac{n\beta}{2}\cos(2\lambda - 3\lambda' + \Omega) + \dot{I}_{drag} \quad (29b)$$

$$\frac{d\Omega}{dt} = \frac{n\beta}{2i}\sin(2\lambda - 3\lambda' + \Omega) + \dot{\Omega}_{sec}, \quad (29c)$$

where $\dot{\Omega}_{sec}$ is the nearly constant secular precession rate arising from electromagnetic and gravitational forces; its presence slightly alters the physical location of resonance. Drag terms influence each of Eqs. (29a)–(29c), but contributions to $d\Omega/dt$ are neglected as they are dominated by $\dot{\Omega}_{sec}$. Finally, the limited radial extent of the resonance zone justifies treating $\dot{n}_{drag}$ as a constant. The resonance strength,

$$\beta \approx \frac{\sqrt{10}L}{2}\left(\frac{(g_{3,3}^2 + h_{3,3}^2)^{1/2}}{g_{1,0}}\right)\left(\frac{R_p}{a}\right)^2 \approx (0.05)L, \quad (30)$$

is one-third of the dn/dt coefficient taken from the $(g_{3,3}: \Psi = 2\lambda - 3\lambda' + \Omega)$ entry of Table II. In the final approximation, we have used parameters appropriate for the jovian 3 : 2 resonance, namely $g_{1,0} \approx 4.218$ G, $g_{3,3} \approx -0.231$ G, $h_{3,3} \approx -0.294$ G (Acuña *et al.* 1983), and $a/R_p \approx 1.7$. At Jupiter, a micrometer-sized grain charged to a potential of +5V, has $L \approx 0.028$ and hence $\beta \approx 0.0014$, a value orders of magnitude greater than typical SGR strengths. Furthermore, since drag forces act on small particles much faster than tidal forces influence large ones, evolution of dust particles in Lorentz resonances proceeds correspondingly more rapidly.

To improve our calculation of β, we would need to include additional contributions from the $g_{j,3}$ and $h_{j,3}$ ($j = 5, 7, 9, \ldots$) field coefficients, but unfortunately, the values of these coefficients are unknown for all nonterrestrial magnetic fields. Nevertheless, we can get a rough upper bound on the error in β by assuming that the higher-order field coefficients are roughly equal in magnitude to the octupole coefficients [for the terrestrial magnetic field, the coefficients decrease in magnitude with increasing order—(Stern 1976)]. In this case, the higher-order terms contribute $\lesssim 0.5\beta$ to the resonance strength. There are also terms in Eqs. (29a)–(29c) that depend on larger powers of e and i, but these contributions amount to $\lesssim 0.1\beta$ for conditions present in the jovian ring.

Finally, we note that the structure of Eqs. (29a)–(29c) is appropriate for all first-order inclination resonances; only the constant coefficients in each equation differ from one resonance to the next (Table II). Second-order (Nth-order) resonances differ only in that the power of i in each of the dn/dt, di/dt, and $d\Omega/dt$ equations is one $(N - 1)$ larger. The $(g_{4,3}: \Psi = 5\lambda - 3\lambda' - 2\Omega)$ and $(g_{4,3}: \Psi = \lambda - 3\lambda' + 2\Omega)$ entries of Table II are each second-order inclination resonances; their positions relative to Jupiter

are given in Fig. 3. Eccentricity resonances of all orders are identical in form to inclination resonances if all i's are replaced by e's, and all Ω's by ϖ's. Because all of these different types of resonances have a similar structure, we expect the same type of dynamic behavior at each of them.

4.2. Resonance Trapping

What happens to particles that drift into resonance? The question is most exactly treated by transforming Eqs. (29a)–(29c) into canonical variables from which a pendulum-like Hamiltonian can be defined (cf. Peale 1976). Such an analysis shows that for an isolated resonance there are two possibilities depending on the direction from which the resonance is approached: resonance trapping and resonant jumps. A trapping probability, which depends on the relative strengths of the resonance and the drag force, is associated with the former. Unfortunately, the Hamiltonian results are awkward to interpret in terms of the orbital elements, the variables that have geometric meaning. Accordingly, the purpose of this and the following section is to give simple descriptions and approximate formulae in terms of orbital elements without resorting to a Hamiltonian analysis. In so doing, we further emphasize the similarities between SGRs, PGRs, and LRs.

When a particle enters the resonance zone and subsequently is stable against perturbations that attempt to dislodge it, the particle is said to have been trapped into resonance. For the particle to remain trapped, its orbital period must stay nearly commensurate with the forcing period, and hence the average value of dn/dt must be zero. This can occur only when the first term in Eq. (29a) balances the second. Thus very large drag rates preclude trapping or, put another way, for a given drag rate many resonances, especially higher-order ones, are too weak to trap passing particles. In Fig. 4, we show what happens to a grain that encounters the 3 : 2 inclination resonance while slowly drifting toward synchronous orbit. Resonant perturbations stop the evolution of the mean motion and simultaneously cause the inclination to grow. The latter growth can be easily explained with the energy constraint, Eq. (27).

Although drag forces themselves need not produce changes in the orbital elements that satisfy Eq. (27) (resonant charge variations are an exception and will be discussed separately below), the resonant portion of the perturbation must. Since the cumulative perturbations for n, e, and i are written as sums of resonant and drag terms (Eqs. (29a) and (29b)), we solve for the resonant terms and substitute these into Eq. (27). The energy constraint takes the form

$$e\frac{de}{dt} + i\frac{di}{dt} = \frac{\dot{n}_{\text{drag}}}{3n}\left(1 - \frac{n}{\Omega_p}\right) + e\dot{e}_{\text{drag}} + i\dot{I}_{\text{drag}}. \quad (31)$$

As it stands, Eq. (31) is directly applicable to mixed resonances (all of the second-order resonances with $g_{j,k}$ coefficients satisfying $j + k$ = odd), which influence both e and i. For nearly circular orbits at inclination resonances, however, eccentricities are only weakly perturbed and can usually be ignored. Furthermore, drag forces typically do not strongly affect orbital inclinations so the $\dot{I}_{\text{drag}}$ term can be dropped. Taking these approximations yields

$$i\frac{di}{dt} = \frac{\dot{n}_{\text{drag}}}{3n}\left(1 - \frac{n}{\Omega_p}\right), \quad (32)$$

which can be directly integrated to

$$i = \sqrt{i_0^2 + \frac{2\dot{n}_{\text{drag}}t}{3n}\left(1 - \frac{n}{\Omega_p}\right)}, \quad (33)$$

where i_0 is the initial inclination and $t = N_p(2\pi/\Omega_p)$ is time, with N_p as the number of jovian rotations (cf. Hamilton and Burns (1993)). The prediction of Eq. (33) agrees well with the numerical integration of Eqs. (29a)–(29c) presented in Fig. 4. We note that Eqs. (32) and (33) are applicable to inclination resonances of all orders and that similar expressions apply to nearly planar orbits at eccentricity resonances. Incidentally, Eq. (32) can also be obtained directly for the 3 : 2 inclination resonance by setting $dn/dt = 0$ in Eqs. (29a)–(29c) and solving for $i\,di/dt$.

As an interesting aside, consider the case where resonant charge variations cause evolution through a Lorentz resonance. Because this drag force is entirely electromagnetic, the full perturbation satisfies Eq. (27). If a particle becomes trapped in a resonance, then dn/dt is zero and hence $e\,de/dt + i\,di/dt = 0$. Thus there can be no secular increase in one of these elements without a corresponding decrease in the other.

Equation (31) shows that particles trapped in resonances systematically change their inclinations and/or eccentricities. Evolution toward synchronous orbit makes i increase while evolution in the opposite sense causes it to decrease (Eq. (33)). Because Eq. (33) gives nonsensical results for shrinking inclinations (the quantity inside the square root becomes negative), particles drifting away from synchronous orbit cannot stay in resonance forever. In fact, by linearizing Eqs. (29a)–(29c) around the equilibrium inclination, it can be shown that solutions in which i decreases are unstable and so particles do not become trapped at all. Conversely, when drifts are toward synchronous orbit, i increases and the linearization yields stable solutions—at least as long as i is small enough for Eqs. (29a)–(29c) to be applicable.

Thus we find that trapping into pure inclination-type and eccentricity-type SGRs, PGRs, or LRs occurs only when drifts are toward the synchronous location (Fig. 3);

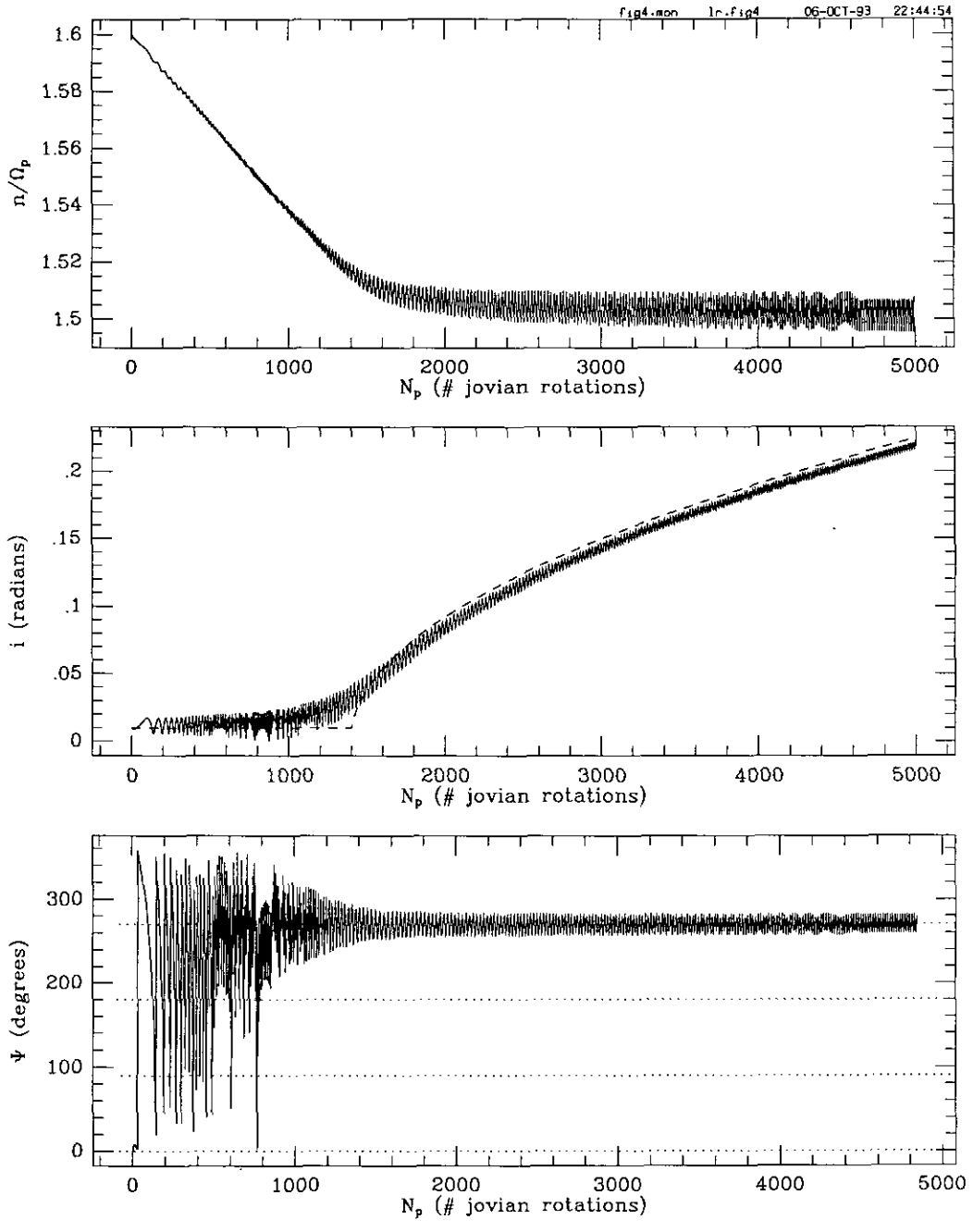

FIG. 4. Resonance trapping. A plot of the orbital evolution numerically determined by Eqs. (29a)–(29c) for jovian parameters $\beta = 1.4 \times 10^{-3}$ and $\dot{n}_{\text{drag}} = -10^{-5}\Omega_p^2$. Plotted against N_p, the number of jovian rotations, are the mean motion ratio n/Ω_p, the inclination i, and the resonant angle Ψ. Initial conditions are $n_0 = 1.6\Omega_p$, $i_0 = 0.01$, and $\Psi_0 = 0$. The resonant angle Ψ librates with small amplitude around a value slightly less than 270° as could have been anticipated by setting Eq. (29a) to zero and solving for Ψ. The dashed curve comes from Eq. (33) which, for these parameters and $N_p \gtrsim N_0 + 100$, is $i \approx 0.0037(N_p - N_0)^{1/2}$. It has been offset slightly to the left (by the choice $N_0 = 1400$) for clarity. Integrations of the full equations of motion, both for SGRs (cf. Fig. 11 of Dermott *et al.* 1988) and for LRs (Hamilton, unpublished), show behavior qualitatively similar to this.

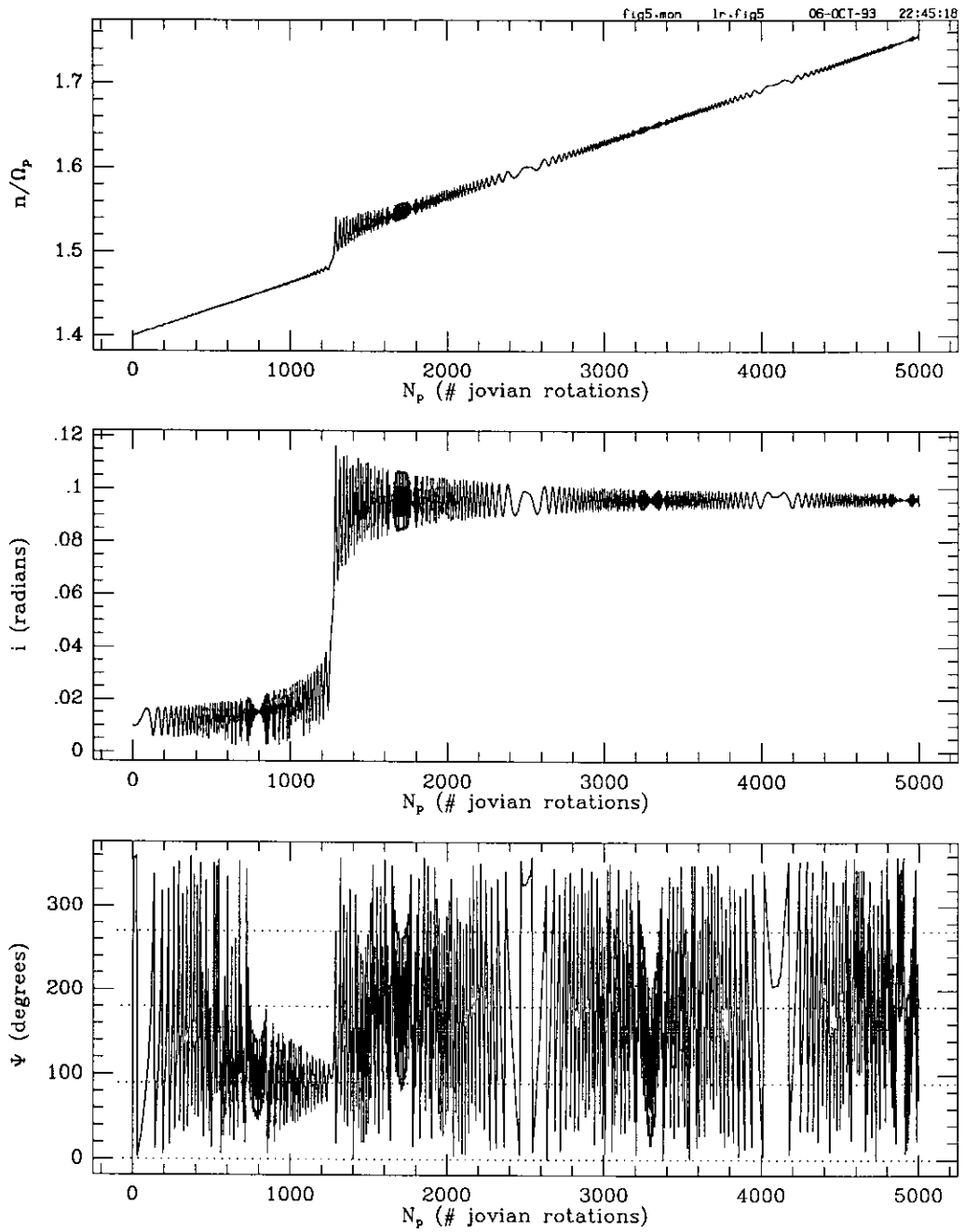

FIG. 5. Jumps at resonance. A plot of the orbital evolution by Eqs. (29a)–(29c) with parameters appropriate for a 1-μm grain: $\beta = 1.4 \times 10^{-3}$; $\dot{n}_{\text{drag}} = 10^{-5}\Omega_p^2$. Initial conditions are $n_0 = 1.4\Omega_p$, $i_0 = 0.01$, and $\Psi_0 = 0$. Notice that the jumps in mean motion (semimajor axis) and inclination occur simultaneously near $n \sim 3\Omega_p/2$ as required by Eq. (34). The resonant argument Ψ librates around a value near 90° until passage through the resonance occurs, after which it circulates. Integrations of the full equations of motion, both for SGRs (cf. Fig. 5 of Dermott *et al.* 1988) and LRs (Hamilton, unpublished), show behavior qualitatively similar to this.

in such cases, the energy integral Eq. (27) requires that there be an associated "square root" growth in e or i (Eq. (33) and Fig. 4).

4.3. Jumps at Resonance

When drifts are away from synchronous orbit, or when the drag rate is too high for resonant trapping to occur, discrete jumps in the inclination (or eccentricity) happen instead. In this section we discuss the mechanism that leads to resonant jumps and derive a simple expression to approximate the jump amplitude in the limiting case of low e and i, and slow drag (cf. Hamilton and Burns 1993).

Figure 5 shows the orbital history of a dust grain drifting away from synchronous orbit and through the jovian 3 : 2

inclination resonance. Far from resonance, the angle Ψ is seen to circulate rapidly and the resonance has little influence on the motion of an orbiting dust particle. As drags bring the particle closer to resonance, however, Ψ starts librating about a value near 90°; because of their cos Ψ dependence, however, dn/dt and di/dt are still not strongly perturbed (Eqs. (29a) and (29b)). Eventually, the equilibrium point about which libration occurs becomes unstable (one can solve for the point at which this occurs from Eqs. (29a)–(29c)). The resonance variable Ψ drifts away from 90°, and resonant perturbations to dn/dt overwhelm the drag force, quickly pushing orbits across the resonance zone. At this point Ψ starts circulating rapidly in the opposite sense, resonant perturbations dwindle in strength, and drag forces dominate orbital evolution once again.

It is clear from Fig. 5 that both n and i experience jumps during passage through resonance. Since the jumps are caused by resonant forces, their magnitudes are necessarily related by Eq. (27). In particular, for inclination resonances, eccentricities are unaffected and so

$$i\,di = -\left(\frac{dn}{3n}\right)\left(1 - \frac{n}{\Omega_p}\right), \tag{34}$$

where dn and di are the jump amplitudes; the former can be approximated simply from the width of the region over which resonant perturbations are significant, which we estimate to be roughly the resonance's libration width. We obtain the libration width by setting $d\Psi/dt = 0$ and using Eqs. (29a)–(29c) to solve separately for the largest possible mean motion (n_{max}) and the smallest (n_{min}); the libration width is then simply $|dn| \approx n_{max} - n_{min}$. For grains drifting away from synchronous orbit through a first-order inclination resonance, we find the mean motion jump,

$$dn \approx -\frac{2n\beta}{i}\left|1 - \frac{n}{\Omega_p}\right|\left(1 - \frac{n}{\Omega_p}\right), \tag{35}$$

which, combined with Eq. (34), yields the inclination jump,

$$di \approx \frac{2\beta}{3i^2}\left|1 - \frac{n}{\Omega_p}\right|^3. \tag{36}$$

As they stand, these expressions are ambiguous since it is unclear what value i has. For nearly circular orbits that drift into strong first-order resonances, however, $di \approx i_f$, where i_f is the inclination immediately after the jump. We approximate the inclination during resonant passage with $i \approx i_f/2 \approx di/2$, which allows us to express each jump amplitude purely as a function of the resonance's location and strength:

$$di \approx 2\left(\frac{\beta}{3}\right)^{1/3}\left|1 - \frac{n}{\Omega_p}\right|, \tag{37}$$

$$dn \approx -2n(3\beta^2)^{1/3}\left(1 - \frac{n}{\Omega_p}\right). \tag{38}$$

As usual, the above discussion applies equally well to all first-order eccentricity resonances. Applying Eqs. (38) and (37) to our jovian example and taking the appropriate parameters from Fig. 5's caption, we estimate $dn = 0.03\Omega_p$ and $di = 0.08$, values lower than, but in reasonable agreement with, the numerically determined jumps observed in Fig. 5. We have also verified the functional dependence of di on β and $1 - n/\Omega_p$ in additional numerical experiments. The numerically determined final inclination in Fig. 5 is ≈5.5° which corresponds to particles rising ≈10,000 km above the jovian equatorial plane, a value in agreement with the ring's observed half-thickness of 8000–10,000 km measured by Showalter *et al.* (1987). Thus the vertical thickness of the jovian halo is consistent with micrometer-sized grains drifting inward from the main ring through the 3 : 2 Lorentz first-order inclination resonance.

Here, and in the preceding section, we have demonstrated that when drag forces bring particles to mean-motion resonances, either trapping or resonant jumps can occur. Because the results of a particular encounter depend so strongly on the direction of drag-induced orbital evolution, however, certain resonance–drag combinations manifest only a single type of behavior. For instance, tidal forces typically drive inner satellites toward outer ones and so the most common resonant phenomena for SGRs is trapping (cf. Goldreich 1965). Conversely, at Lorentz resonances, plasma and atmospheric drags cause orbits to evolve away from the synchronous location which leads to resonant jumps. In Table III, we summa-

TABLE III
Results of Resonance-Drag Interactions

Resonance	Drag force	Typical dynamics
SGR	Tidal	Trapping
SGR	Plasma and atmospheric and Poynting–Robertson	Trapping and jumps
PGR[a]	Tidal and plasma and atmospheric	Jumps
PGR	Poynting-Robertson	Trapping and jumps
LR	Tidal	(Incompatible)
LR	Plasma and atmospheric	Jumps
LR	Poynting–Robertson	Trapping and jumps
All	Resonant charge variations	?

[a] Here we have assumed a static gravity field for PGRs which is a good approximation for the terrestrial planets. Since gravitational modes of the giant planets can rotate rapidly (cf. Marley 1991), resonant locations are significantly altered and, hence, both types of dynamical behavior can occur.

rize the typical outcome of couplings between each of the resonances and drag forces discussed above. In all cases, the dynamical outcome of an interaction depends on the direction of drag-induced orbital evolution at a given resonant location, not on the structure of the particular resonance. This serves to reemphasize the fact that resonances arising from very different perturbations are dynamically similar.

5. SUMMARY

In this paper, we present the first disturbing-function-style expansion of the Lorentz force (Table II). Our expansion, which is to second order in eccentricities and inclinations, provides simple equations valid for first-order e and i resonances as well as for second-order e^2, i^2, and ei resonances. To lowest order, our equations for Lorentz resonances have the same form as those derived for gravitational resonances which accounts nicely for the similar dynamical behavior that we have observed in numerical integrations.

We trace many of the similarities between different types of resonances to basic orbital symmetries that constrain the functional form of all quantities—and hence all perturbations—expressed in terms of orbital elements. In particular, these orbital symmetries account for several of the patterns long noticed in expansions of the satellite disturbing function. Additional regularities are due to the fact that the three perturbations considered in this paper—SGRs, PGRs, and LRs—are all constrained by a nearly identical integral of the motion. This integral exists for an arbitrary orbital perturbation provided that a rotating frame can be found in which the perturbation, or at least the resonant part thereof, is independent of time.

Our results imply that the orbital dynamics displayed at mean-motion resonances are fundamental. The first-order structure of a given resonance is determined primarily by orbital symmetries and by the integral of the motion. The character of the perturbing force is important only in determining absolute resonance strengths.

ACKNOWLEDGMENTS

The idea to characterize Lorentz resonances mathematically was originally Joe Burns' and I thank Joe for his encouragement and involvement during all stages of this work. I was also inspired by Carl Murray's eighth-order expansion of the disturbing function and benefited from several interesting discussions with Phil Nicholson. Andrea Milani and Carl Murray provided helpful reviews of the manuscript. This work was supported by NASA Grant NAGW-310.

REFERENCES

ACUÑA, M. H., K. W. BEHANNON, AND J. E. P. CONNERNEY 1983. Jupiter's magnetic field and magnetosphere. In *Physics of the Jovian Magnetosphere* (A. J. Dessler, Ed.), pp. 1–50. Cambridge Univ. Press, New York, NY.

APPLEGATE, J. H., M. R. DOUGLAS, Y. GÜRSEL, G. J. SUSSMAN, AND J. WISDOM 1986. The outer solar system for 200 million years. *Astron. J.* **92,** 176–194.

BORDERIES, N., AND P. GOLDREICH 1984. A simple derivation of capture probabilities for the J + 1 : J and J + 2 : J orbit-orbit resonance problems. *Cel. Mech.* **32,** 127–136.

BROWN, E. W., AND C. A. SHOOK 1993. *Planetary Theory*. Cambridge Univ. Press, Cambridge, UK.

BURNS, J. A., P. L. LAMY, AND S. SOTER 1979. Radiation forces on small particles in the solar system. *Icarus* **40,** 1–48.

BURNS, J. A., AND L. E. SCHAFFER 1989. Orbital evolution of circumplanetary dust by resonant charge variations. *Nature* **337,** 340–343.

BURNS, J. A., L. E. SCHAFFER, R. J. GREENBERG, AND M. R. SHOWALTER 1985. Lorentz resonances and the structure of the jovian ring. *Nature* **316,** 115–119.

D'ALEMBERT, J. L. R. 1754. *Recherches sur différens Points importans du Système du Monde*. Mém. Paris Acad. Sc.

DANBY, J. M. A. 1988. *Fundamentals of Celestial Mechanics* (2nd ed.). Willmann–Bell, Richmond, VA.

DERMOTT, S. F., R. MALHOTRA, AND C. D. MURRAY 1988. Dynamics of the uranian and saturnian systems. A chaotic route to melting Miranda? *Icarus* 76, 295–334.

FRANKLIN, F. A., G. COLOMBO, AND A. F. COOK 1982. A possible link between the rotation of Saturn and its ring structure. *Nature* **293,** 128–130.

GOLD, T. 1975. Resonant orbits of grains and the formation of satellites. *Icarus* **25,** 489–491.

GOLDREICH, P. 1965. An explanation for the frequent occurrence of commensurable mean motions in the solar system. *Mon. Not. R. Astron. Soc.* **130,** 159–181.

GOLDREICH, P., S. TREMAINE, AND N. BORDERIES 1986. Toward a theory for Neptune's arc rings. *Astron. J.* **92,** 490–494.

GONCZI, R., CH. FROESCHLE, AND CL. FROESCHLE 1982. Poynting–Robertson drag and orbital resonance. *Icarus* **51,** 633–654.

GREENBERG, R. 1973a. Evolution of satellite resonances by tidal dissipation. *Astron. J.* **78,** 338–346.

GREENBERG, R. 1973b. The inclination-type resonance of Mimas and Tethys. *Mon. Not. R. Astron. Soc.* **165,** 305–311.

HAMILTON, D. P. 1993. Motion of dust in a planetary magnetosphere: Orbit-averaged equations for oblateness, electromagnetic, and radiation forces with application to Saturn's E ring. *Icarus* **101,** 244–264. [Erratum, *Icarus* **103,** 161]

HAMILTON, D. P., AND J. A. BURNS 1993. Lorentz and gravitational resonances on circumplanetary particles. *Adv. Space Res.* **13**(10), 241–248.

HAMILTON, D. P., J. A. BURNS, AND M. HORANYI 1992. Neptune dust dynamics. In *Neptune and Triton Meeting Abstracts*, pp. 29. Tucson, AZ.

HENRARD, J., 1982. Capture into resonance: An extension of the use of adiabatic invariants. *Cel. Mech.* **27,** 3–22.

HORANYI, M., AND J. A. BURNS 1991. Charged dust dynamics: Orbital resonance due to planetary shadows. *J. Geophys. Res.* **96,** 19283–19289.

HORANYI, M., J. A. BURNS, AND D. P. HAMILTON 1992. The dynamics of Saturn's E ring particles. *Icarus* **97,** 248–259.

JACKSON, A. A., AND H. A. ZOOK 1989. A solar system dust ring with the Earth as its shepherd. *Nature* **337,** 629–631.

JACKSON, A. A., AND H. A. ZOOK 1992. Orbital evolution of dust particles from comets and asteroids. *Icarus* **97,** 70–84.

KAULA, W. M. 1966. *Theory of Satellite Geodesy*. Blaisdell, Waltham, MA.

LAZZARO, D., B. SICARDY, F. ROQUES, AND R. GREENBERG 1993. Is there a planet around β Pictoris? Perturbations of a planet on a circumstellar dust disk. II. The analytical model. *Icarus*, **108,** 37–58.

LEVY, E. H. 1989. Possible time variations of Jupiter's magnetic field. In *Time-Variable Phenomena in the Jovian System*, (M. J. S. Belton, R. A. West, and J. Rahe, Eds.), NASA SP-494, pp. 129–138.

MALHOTRA, R. 1991. Tidal origin of the Laplace resonance and the resurfacing of Ganymede. *Icarus* **94,** 399–412.

MARLEY, M. S. 1991. Nonradial oscillations of Saturn. *Icarus* **94,** 420–435.

MARLEY, M. S., AND C. C. PORCO 1993. Planetary acoustic mode seismology: Saturn's ring. *Icarus* **106,** 508–524.

MESSAGE, P. J. 1991. Perturbation theory, resonance, librations, chaos, and Halley's comet. In *Predictability, Stability, and Chaos in N-Body Dynamical Systems* (A. E. Roy, Ed.), pp. 239–247. Plenum, New York.

MIGNARD, F. 1984. Effects of radiation forces on dust particles in planetary rings. In *Planetary Rings* (R. Greenberg and A. Brahic, Eds.), pp. 333–366. Univ. of Arizona Press, Tucson.

MILANI, A., A. M. NOBILI, AND M. CARPINO 1987. Secular variations of the semimajor axes: Theory and experiments. *Astron. Astrophys.* **172,** 265–279.

MURRAY, C. D., AND D. HARPER 1993. *Expansion of the Planetary Disturbing Function to Eighth Order in the Individual Orbital Elements*. QMW Math Notes No. 15, Queen Mary and Westfield College, Mile End Road, London E1 4NS, UK.

NORTHROP, T. G., D. A. MENDIS, AND L. E. SCHAFFER 1989. Gyrophase drifts and the orbital evolution of dust at Jupiter's gossamer ring. *J. Geophys. Res.* **79,** 101–115.

PEALE, S. J. 1976. Orbital resonances in the solar system. *Annu. Rev. Astron. Astrophys.* **14,** 215–246.

PORCO, C. C. 1991. An explanation for Neptune's ring arcs. *Science* **253,** 995–1000.

ROQUES, F., H. SCHOLL, B. SICARDY, AND B. SMITH 1993. Is there a planet around β Pictoris? Perturbations of a planet on a circumstellar dust disk. I. The numerical simulation. *Icarus*, **108,** 59–80.

ROY, A. E. 1978. *Orbital Motion*. Hilger, Bristol, UK.

SCHAFFER, L. E., AND J. A. BURNS 1987. The dynamics of weakly charged dust: Motion through Jupiter's gravitational and magnetic fields. *J. Geophys. Res.* **92,** 2264–2280.

SCHAFFER, L. E., AND J. A. BURNS 1992. Lorentz resonances and the vertical structure of dusty rings: Analytical and numerical results. *Icarus* **96,** 65–84.

SHOWALTER, M. R., J. A. BURNS, J. N. CUZZI, AND J. B. POLLACK 1985. Jupiter's gossamer ring *Nature* **316,** 526–528.

SHOWALTER, M. R., J. A. BURNS, J. N. CUZZI, AND J. B. POLLACK 1987. Jupiter's ring system: New results on structure and particle properties. *Icarus* **69,** 458–498.

SHOWALTER, M. R., J. N. CUZZI, AND S. M. LARSON 1991. Structure and particle properties of Saturn's E ring. *Icarus* **94,** 451–473.

SINCLAIR, A. T. 1975. The orbital resonance amongst the Galilean satellites of Jupiter. *Mon. Not. R. Astron. Soc.* **171,** 59–72.

SMART, W. M. 1953. *Celestial Mechanics*. Cambridge Univ. Press. Cambridge, UK.

STERN, D. P. 1976. Representation of magnetic fields in space. *Rev. Geophys. Space Phys.* **14,** 199–214.

WEIDENSCHILLING, S. J., AND A. A. JACKSON 1993. Orbital resonances and Poynting–Robertson drag. *Icarus* **104,** 244–254.

WISDOM, J. 1980. The resonance overlap criterion and the onset of stochastic behavior in the restricted three-body problem. *Astron. J.* **85,** 1122–1133.

YODER, C. F. 1982. Tidal rigidity of Phobos. *Icarus* **49,** 327–346.